BioRxiv

Undinarchaeota illuminate the evolution of DPANN archaea

Nina Dombrowski[1], Tom A. Williams[2], Jiarui Sun[3], Benjamin J. Woodcroft[3], Jun-Hoe Lee[4], Bui Quang Minh[5], Christian Rinke[3], Anja Spang[1,5,#]

[1]NIOZ, Royal Netherlands Institute for Sea Research, Department of Marine Microbiology and Biogeochemistry, and Utrecht University, P.O. Box 59, NL-1790 AB Den Burg, The Netherlands
[2] School of Biological Sciences, University of Bristol, Bristol, BS8 1TQ, UK
[3]Australian Centre for Ecogenomics, School of Chemistry and Molecular Biosciences, The University of Queensland, QLD 4072, Australia
[4]Department of Cell- and Molecular Biology, Science for Life Laboratory, Uppsala University, SE-75123, Uppsala, Sweden
[5]Research School of Computer Science and Research School of Biology, Australian National University, ACT 2601, Australia

#corresponding author. Postal address: Landsdiep 4, 1797 SZ 't Horntje (Texel). Email address: anja.spang@nioz.nl. Phone number: +31 (0)222 369 526

Introductory paragraph

The evolution and diversification of Archaea is central to the history of life on Earth. Cultivation-independent approaches have revealed the existence of at least ten archaeal lineages whose members have small cell and genome sizes and limited metabolic capabilities and together comprise the tentative DPANN archaea. However, the phylogenetic diversity of DPANN and the placement of the various lineages of this group in the archaeal tree remain debated. Here, we reconstructed additional metagenome assembled genomes (MAGs) of a thus far uncharacterized archaeal phylum-level lineage UAP2 (*Candidatus* Undinarchaeota) affiliating with DPANN archaea. Comparative genome analyses revealed that members of the Undinarchaeota have small estimated genome sizes and, while potentially being able to conserve energy through fermentation, likely depend on partner organisms for the acquisition of vitamins, amino acids and other metabolites. Phylogenomic analyses robustly recovered Undinarchaeota as a major independent lineage between two highly supported clans of DPANN: one clan comprising Micrarchaeota, Altiarchaeota and Diapherotrites, and another encompassing all other DPANN. Our analyses also suggest that DPANN archaea may have exchanged core genes with their hosts by horizontal gene transfer (HGT), adding to the difficulty of placing DPANN in the archaeal tree. Together, our findings provide crucial insights into the origins and evolution of DPANN archaea and their hosts.

Introduction

Archaea represent one of the two primary domains of life[1–3] and are thought to have played a major role in the evolution of life and origin of Eukaryotes[4–6]. While most archaea remain uncultivated, cultivation-independent approaches, such as single-cell and metagenomic sequencing, have revealed many previously unknown archaeal lineages in most environments on Earth and have changed our perception of archaeal functional and taxonomic diversity[7–10]. In particular, the Asgard[6] and DPANN superphyla[11,12] as well as a multitude of putative phylum-level lineages have been proposed in the archaeal domain over the last two decades but the phylogenetic relatedness and taxonomy of different archaeal lineages remain a matter of debate.

The DPANN radiation[12], named after the first members of this group (Diapherotrites, Parvarchaeota, Aenigmarchaeota, Nanoarchaeota and Nanohaloarchaeota)[11], comprises one of these recently proposed archaeal clades and is now thought to be comprised of at least ten and (according to NCBI taxonomy) putative phylum-level lineages[13,14]. Most members of the DPANN archaea are characterized by small cell sizes and reduced genomes, which code for a limited set of metabolic proteins[13]. The few members that have been successfully enriched in co-culture were shown to represent obligate ectosymbionts dependent on archaeal hosts for growth and survival. For instance, members of Nanoarchaeota are ectosymbionts of TACK archaea[15–20], Micrarchaeota were found in co-culture with Thermoplasmates[21,22] and Nanohaloarchaeota are dependent on halobacterial hosts[23]. Furthermore, evidence from FISH and co-occurrence analyses have suggested that Huberarchaeota may be ectosymbionts of members of the Altiarchaeota[24,25]. Yet, for most DPANN representatives, the identity of their symbiotic partners remains unclear.

Ever since the discovery of the first DPANN representative - *Nanoarchaeum equitans,* an ectosymbiont of *Ignicoccus hospitalis*[15] - the phylogenetic placement of putative DPANN clades in the archaeal tree have been uncertain[26]. While various phylogenetic analyses have indicated that DPANN may comprise a monophyletic radiation in the Archaea[10,11,27], these have been debated[8,28,29]. In particular, analyses focusing on the placement of selected DPANN lineages in isolation, such as Nanoarchaeota and Parvarchaeota, relative to other Archaea, have led to the conclusion that these represent fast-evolving Euryarchaeota[28,29]. Furthermore, it is debated whether the free-living Altiarchaeota belong to the DPANN radiation, form an independent lineage or belong to Euryarchaeota[8,9,14,30,31]. A potential cause for these conflicting topologies is that DPANN are often found on long branches in phylogenetic trees; these long branches might result from compositional biases or fast evolutionary rates[32,33] (as seen for obligate bacterial endosymbionts[34,35]) or might reflect genomic under sampling of the true diversity of this group[9]. These alternatives are difficult to distinguish because, in the absence of fossils or definitive geochemical traces in the fossil record, we lack a well-constrained timescale for archaeal evolution. Distantly-related long-branching lineages can sometimes artificially group together on trees due to methodological artefacts, a phenomenon called long ranch attraction (LBA)[32]. Ways to ameliorate such artifacts include increased taxonomic sampling[36], use of phylogenetic models less prone to LBA[37], and the removal of fast-evolving or compositionally-biased sites from the alignment[38]. Furthermore, it seems possible that horizontal gene transfers (HGT) between symbionts and hosts[39] could impede correct phylogenetic inferences if not accounted for.

77 Several recent studies have revealed the presence of a thus far uncharacterized archaeal lineage
78 referred to the Uncultivated Archaeal Phylum 2 (UAP2)[13,40,41], which seems to affiliate with DPANN
79 archaea and thus may be key in resolving long-standing debates regarding archaeal phylogeny and the
80 evolution of DPANN. In this study, we have used a metagenomics approach to obtain additional genomes
81 of members of the so far uncharacterized UAP2 and provide first insights into their metabolic repertoire
82 and lifestyle. Furthermore, we implemented comprehensive and careful phylogenomic techniques aimed
83 at ameliorating phylogenetic artifacts, shedding new light onto the evolutionary origin and phylogenetic
84 placement of the various DPANN lineages including UAP2 in an updated archaeal phylogeny.

85 Results and Discussion

86 **A thus far uncharacterized putative archaeal phylum-level lineage in metagenome read archives**

87 The generation of a large diversity of metagenome-assembled genomes (MAGs) representing
88 archaeal and bacterial lineages across the tree of life has led to the definition of the tentative archaeal
89 UAP2 phylum[41]. Considering our lack of insights into the biology of members of this lineage as well as its
90 suggested key position in the archaeal tree, we aimed at obtaining a broader genomic representation of
91 the UAP2. In particular, we screened publicly available metagenomes using ribosomal protein sequences
92 of the previously reconstructed UAP2 MAGs and assembled and binned UAP2-positive samples yielding
93 six additional MAGs belonging to the UAP2 lineage (**Table 1, Supplementary Tables 1-2,** see Methods for
94 details). Four of the newly assembled MAGs were recovered from metagenomes of a groundwater aquifer
95 located adjacent to the Colorado River[42], while the two others as well as six previously reconstructed
96 MAGs, derived from metagenomes of marine waters in the Atlantic[41,43] and Indian Oceans[44] as well as the
97 Mediterranean Sea[45] (**Supplementary Table 2**). UAP2 representatives were detected in samples from
98 various depths in the water column (85-5000 m), fluctuating oxygen conditions (anoxic to oxic) and
99 temperatures (sampling sites had temperatures from 18 up to 106°C) (**Supplementary Figure 1,**
100 **Supplementary Table 1**). The MAGs, including previously published ones, are on average 78% complete
101 (min: 55%, max: 91%) and show low signs of contamination (<5%) and strain heterogeneity (<2%). In total,
102 they represent 2 high-quality (one from this study) and 10 medium-quality draft genomes according to
103 genome reporting standards for MAGs assessed using a general archaeal marker protein set (**Table 1,**
104 Supplementary Information)[46]. The UAP2 MAGs have small genomes with an average size of 0.66 MB,
105 coding for an average of 750 proteins. They likely represent a distinct archaeal phylum-level lineage based
106 on average amino acid identity (AAI) comparisons with other archaeal taxa (**Supplementary Figure 2**,
107 **Supplementary Table 3**), phylogenetic analyses including a concatenated 16S-23S rRNA gene tree
108 (**Supplementary Figures 3-5** and see below) as well as classification based on the Genome Taxonomy
109 Database (GTDB) rank normalization (**Table 1, Supplementary Table S2**). Furthermore, the aquifer and
110 marine UAP2 MAGs likely represent different orders as suggested by a relative evolutionary divergence
111 (RED) value of 0.47[47]. Based on two high-quality UAP2 MAGs (Table 1, **Supplementary Table S2**)[46], we
112 propose two type species; *Candidatus* Undinarchaeum marinum (SRR4028224.bin17) and *Candidatus*
113 Naiadarchaeum limnaeum (SRR2090159.bin1129), representing the marine and aquifer UAP2 clade,
114 respectively (see details below). Undines are water elementals described in the writings of the alchemist
115 Paracelsus, while Naiads were nymphs residing in ponds, springs and other bodies of fresh water in Greek
116 mythology.

117
118 **Undinarchaeota branch between two major DPANN clades**
119 Initial phylogenetic analyses placed Undinarchaeota (formerly UAP2) as a sister lineage to all other
120 DPANN archaea in unrooted trees[13,14,41]. If correct, this placement could give important insights into the
121 timing of DPANN evolution and the nature of the putative last DPANN common ancestor. However, this
122 deep-branching position was poorly supported[13,41]. In order to resolve the phylogenetic relationship of
123 Undinarchaeota and DPANN archaea as well as to test the monophyly of the DPANN radiation, we
124 performed in-depth phylogenetic analyses.
125 We began by updating the taxon sampling in three published marker protein datasets[10,48,49] and
126 inferred single-protein trees for each marker to evaluate phylogenetic congruence and detect
127 contaminant sequences and HGTs. Since initial manual inspection revealed extensive incongruence
128 among markers, we developed a marker protein ranking scheme to compare proteins and datasets
129 systematically and without a priori assumptions regarding archaeal phylogeny above the rank of order-,
130 class- or phylum. Briefly, we ranked marker genes according to the extent to which they supported the
131 monophyly of well-established archaeal phylum-, class and order-level lineages (**Supplementary Tables**
132 **4-5)** (Methods, Supplementary Information)[6,48,49]. For example, low ranking makers were highly
133 incongruent with individual members of accepted lineages not grouping together and had high numbers
134 of so-called splits indicating HGT events (see Methods for details, **Supplementary Tables 4-5**), while top
135 ranked markers had low indications for potential HGTs between specific DPANN lineages and unrelated
136 taxa. Note that since DPANN monophyly remains actively debated[8,9,11,12,26–29], we did not penalize marker
137 genes for failing to recover the monophyly of the superphylum as a whole, i.e. the placement of certain
138 DPANN lineages with other archaeal taxa.
139 These analyses revealed that many universal archaeal genes, including those coding for ribosomal
140 proteins and other core elements of the genetic machinery, may have undergone inter-lineage gene
141 transfers during archaeal diversification (**Supplementary Tables 4-5**). We now have increased power to
142 detect such transfers due to the expanded taxonomic sampling of the archaeal domain compared to
143 previous analyses but the information contained in single protein alignments as well as bootstrap support
144 in corresponding trees is generally low (see Methods**, Supplementary Tables 4-5)**, motivating the use of
145 protein concatenations for phylogenetic reconstructions. However, a large number of gene transfers
146 among markers can mislead phylogenomic analysis because current concatenation and supertree
147 methods assume that all genes evolve on the same underlying tree. To ameliorate the impact of
148 incongruent markers on our inferences, concatenated phylogenies were inferred from the 25% and 50%
149 top-ranked marker proteins which corresponds to those markers with lowest numbers of splits and in turn
150 potential HGTs. We used the best-fitting models of sequence evolution available in both maximum-
151 likelihood using IQ-TREE[50] and Bayesian frameworks[51], in combination with alignment recoding,
152 assessment and filtering of compositional biases, as well as statistical topology testing (**Supplementary**
153 **Table 6, Supplementary Figures 6-56,** Methods, Supplementary Information). Our analyses consistently
154 recovered the clanhood[52] of the DPANN archaea (including Undinarchaeota) as a whole (that is, all DPANN
155 archaea clustered together on the unrooted tree). Furthermore, our inferences based on curated marker
156 set alignments suggested that Undinarchaeota form a distinct lineage that branches between two other
157 DPANN clans (sequence clusters on the unrooted tree[52]) with maximum statistical support (**Figure 1a,b,**
158 **Supplementary Figures 6-45, Supplementary Table 6**; Supplementary Information). These clans

159 comprised the Altiarchaeota, Micrarchaeota and Diapherotrites (hereafter referred to as DPANN Cluster
160 1) and all remaining members of the DPANN (Woesearchaeota, Pacearchaeota, Parvarchaeota, UAP1,
161 Nanoarchaeota, Huberarchaeota, Aenigmarchaeota and Nanohaloarchaeota) (hereafter referred to as
162 DPANN Cluster 2), respectively (**Figure 1a,b**). Finally, in all phylogenies, Undinarchaeota formed two
163 GTDB-level orders, consisting of aquifer-derived and ocean-derived MAGs, i.e. the Naiadarchaeales and
164 Undinarchaeales, respectively (**Figure 1a,b; Supplementary Table 2**).

165 Next, we compared these results with phylogenetic inferences based on the 25 and 50% most
166 incongruent markers (**Supplementary Tables 4-5**), which were inferred to have experienced high rates of
167 inter-lineage transfers or were otherwise affected by conflicting phylogenetic signals (**Supplementary**
168 **Figures 46-49)**. In agreement with our predictions, these analyses yielded phylogenetic trees with various
169 highly supported clusters among unrelated taxa (Supplementary Information). For instance, analyses
170 based on the 25% lowest ranking markers recovered Nanoarchaeota as members of the TACK archaea
171 (**Supplementary Figure 47**) and Nanohaloarchaeota as a sister lineage of Halobacteria (either as a
172 separate cluster (**Supplementary Figure 46**) or with DPANN archaea (**Supplementary Figure 47)**, in
173 agreement with known symbiont-host relationships[16,17,23]. This is particularly notable because we did not
174 a priori penalize trees in which certain DPANN lineages branch with certain other archaeal lineages
175 (**Supplementary Tables 4-5**). In turn, these analyses suggest that conflicting results regarding the
176 placement of certain DPANN lineages, may be due to, at least in part, to the use of a large number of
177 markers affected by host-symbiont HGT. For instance, Nanohaloarchaeota may artificially be drawn
178 towards the Euryarchaeota[28] when marker sets include too many proteins that were affected by
179 symbiont-host transfers.

180 Compositional biases in protein sequences can also lead to artefacts in phylogenetic
181 reconstructions[53,54]. To assess the reliability of the inferred placement of Undinarchaeota based on our
182 top-ranked marker protein sets and to ameliorate remaining biases, we subjected the curated alignment
183 to different data treatments including removal of compositionally heterogeneous and fast-evolving sites
184 (see Methods for details, **Supplementary Table 6, Supplementary Figures 13-22 and 30-40**). Removal of
185 compositionally biased sites resulted in notable changes in the tree topology. In particular, the originally
186 inferred sister relationship between Haloarchaea and Methanonatronarchaeia[55] was supported only in
187 analyses based on the original non-treated alignment; removal of 10% or more of the most biased sites
188 instead supported a close relationship between Methanonatronarchaeia and Archaeoglobales
189 (**Supplementary Figures 13 and 17**), in agreement with more recent work[56]. Importantly, the placement
190 of Undinarchaeota relative to the DPANN Cluster 1 and Cluster 2, as well as the monophyly of each of
191 these clusters, remained stable irrespective of the fraction of heterogeneous sites removed (10% - 40% of
192 sites), suggesting that our inferences are not an artifact of compositional biases.

193 Finally, we reconstructed phylogenies using a recently-developed non-reversible substitution
194 model that captures asymmetries in the exchange rates between amino acids[57] to investigate the position
195 of Undinarchaeota relative to the root of the archaeal tree (**Figure 1c, Supplementary Figures**
196 **10,11,19,22,24,25,36 and 39, Supplementary Table 6**). This method does not rely on an outgroup and
197 therefore avoids potential LBA artifacts associated with the use of distantly related bacterial sequences
198 to root the archaeal tree[27]. Notably, all our analyses recovered a monophyletic clade of Asgard, TACK and
199 Euryarchaeota with the root being excluded from within this clade with high statistical support (100%).
200 However, the non-reversible model failed to strongly resolve the root position within the DPANN

201 radiation. In particular, the maximum-likelihood root was placed either (a) between all DPANN (including
202 Cluster 1 and 2 as well as Undinarchaeota) on one side and all other Archaea on the other side (**Figure**
203 **1c,d, Supplementary Table 6, Supplementary Figures 10-11**), (b) between the Cluster 1 and all other
204 archaea (**Figure 1e, Supplementary Table 6, Supplementary Figures 24-25 and 36**) or(c) between a cluster
205 comprising Micrarchaeota-Diapherotrites and the rest of the Archaea (**Figure 1f, Supplementary Table 6,**
206 **Supplementary Figures 19, 22 and 39**). However, none of these root positions inferred using non-
207 reversible models received high bootstrap support. Rooting using a bacterial outgroup recovered a root
208 between a monophyletic DPANN clade and the rest of Archaea with moderate to high bootstrap support
209 (94% ultrafast bootstrap[58], 98% SH-like aLRT support[59]; **Supplementary Figure S56**), consistent with
210 previous results[27]. Thus, our analyses provide strong support for the clanhood of DPANN archaea including
211 Undinarchaeota, but do not confidently resolve the position of the archaeal root either within that clan,
212 or between DPANN and other Archaea[10,14,27].
213
214 **Synapomorphies supporting the monophyly of Undinarchaeota and Cluster 2 DPANN**
215 To further assess the phylogenetic placement of the Undinarchaeota lineage, we surveyed the
216 genomes of DPANN lineages for gene content synapomorphies (shared derived characters) that might
217 enable us to distinguish competing hypotheses for the archaeal root. Similar to other DPANN lineages,
218 Undinarchaeota MAGs encode most proteins involved in replication, transcription and translation and
219 repair (**Supplementary Tables 7-9**, **Supplementary Figures 58-61**, Supplementary Information). While
220 Undinarchaeota did not share specific features with any of the other archaeal clades, we identified
221 candidate synapomorphies supporting a monophyletic clade comprising Undinarchaeota and Cluster 2
222 DPANN. Specifically, members of these lineages lack genes encoding the exosome component Csl4, which
223 is present in Cluster 1 DPANN and most other archaea (**Supplementary Figure 61**). The archaeal exosome
224 is thought to consist of four subunits: Rrp41 and Rrp42 form the core ring structure, and Csl4 and Rrp4
225 constitute the rRNA-binding cap[60]. In spite of the absence of Csl4, Undinarchaeota and Cluster 2 DPANN
226 archaea encode all other subunits of the complex (Rrp4/41/42) suggesting a structural or functional
227 difference of their exosome.
228 Furthermore, Undinarchaeota and Cluster 2 DPANN share a synapomorphy related to the
229 archaeal DNA primase[61]. Previous work[62] has suggested that, while DNA primases of most Archaea
230 (including those of the Micrarchaeota) are composed of two subunits encoded by *pri*S and *pri*L, some
231 DPANN lineages (at that time the Nanoarchaeota, Nanohaloarchaeota and Parvarchaeota), were found to
232 possess a *pri*S-*pri*L fusion gene. Our analyses, which includes a larger genomic representation of DPANN
233 archaea, revealed that representatives of the DPANN Cluster 1 consistently encode canonical *pri*S and *pri*L
234 genes, while all Undinarchaeota and DPANN Cluster 2 archaea have a fused version (**Supplementary Table**
235 **11**). Note that *pri*S and *pri*L arose from an ancestral duplication and are thus homologous. A phylogenetic
236 analysis of all PriS and PriL subunits (after splitting the fused version), revealed that the fusion likely
237 occurred at the origin of the Undinarchaeota and DPANN Cluster 2 (100/100 and 91.3/99 bootstrap
238 support for PriS and PriL, respectively; **Supplementary Figure 57**).
239 Consistent with our phylogenetic analyses, these findings support a clade containing
240 Undinarchaeota and DPANN Cluster 2 as sister lineages from which the archaeal root is excluded. It will
241 be interesting to experimentally investigate the functional implication of the identified synapomorphies

242 (exosome component loss, DNA primase fusion) and determine whether they could have played a role in
243 reductive genome evolution in Undinarchaeota and DPANN Cluster 2 archaea.
244
245 **Gene repertoires indicate fermentative lifestyle and reliance on a host**
246 *Catabolism.* Comparative genome analyses and inference of the metabolic potential of
247 Undinarchaeota (**Supplementary Tables 7-8 and 12-15,** Supplementary Information for details), suggest
248 that representatives of this clade likely rely on fermentative processes for energy conservation (**Figure 2**).
249 In particular, the presence of the lower Embden-Meyerhof and non-oxidative pentose-phosphate
250 pathway but absence of most genes coding for enzymes of the tricarboxylic acid cycle (TCA) suggest that
251 Undinarchaeota could generate ATP through fermentation of pyruvate to acetate. Simple carbohydrates,
252 such as pyruvate, could perhaps be taken up by passive diffusion[63]. Furthermore, some members of the
253 Naiad- and Undinarchaeales may be able to use extracellular DNA as growth substrates (**Figure 2**). For
254 example, most representatives of the Undinarchaeota encode the complete nucleoside degradation
255 pathway[64–66](Supplementary Information), including an AMP phosphorylase (DeoA), ribose 1,5-
256 bisphosphate isomerase and Group-III ribulose 1,5-bisphosphate carboxylase (RbcL; RuBisCO)
257 (**Supplementary Figure 59**). In fact, many DPANN representatives have been reported to harbor a RuBisCO
258 homolog and certain members have been suggested to be able to use nucleosides as substrates[66,67].
259 Undinarchaeota may import DNA via pili encoded by all Undinarchaeota MAGs and subsequently degrade
260 those using their encoded nucleases (Supplementary Information)[68,69]. Intermediates of the nucleoside
261 degradation pathway, such as glycerate-3-phosphate, may subsequently be channeled into the lower
262 glycolytic pathway and contribute to energy conservation by an ATP synthesizing acetate-CoA ligase
263 (acdA). Other products (e.g. glyceraldehyde-3P and fructose-6P produced via gluconeogenesis) may be
264 further metabolized through the non-oxidative pentose-phosphate pathway allowing the synthesis of
265 cellular building blocks such as pyrimidines and purines. It is however notable that group-III-like RuBisCO
266 homologs encoded by Undinarchaeales MAGs have mutations in two positions of the RuBisCO motif[64–67].
267 In turn, it remains to be determined whether RuBisCO has retained its canonical function in these
268 members of the Undinarchaeales and indeed enables growth on nucleosides (**Supplementary Figure 59**;
269 Supplementary Information). Considering the limited set of predicted proteins involved in central carbon
270 metabolism, experimental verification will be needed to assess whether the encoded pathways provide
271 sufficient ATP to sustain the energy metabolism of the various Undinarchaeota representatives.
272 *Anabolism.* Even though all representatives of the Undinarchaeota encode a near complete
273 gluconeogenesis pathway (**Figure 2**) including the potentially ancient bifunctional fructose 1,6-
274 bisphosphate (FBP) aldolase/phosphatase, which would allow the synthesis of fructose-6-phosphate[70],
275 many other biosynthesis pathways are incomplete. For instance, while the Naiadarchaeales MAGs encode
276 all proteins required to synthesize archaeal-type ether lipids, lipid biosynthesis pathways are incomplete
277 in Undinarchaeales MAGs, which lack key genes for the conversion of glycerone-phosphate to
278 archaetidylinosytol-phosphate, in spite of the presence of the archaeal mevalonate pathway[10] in
279 representatives of both lineages. Incomplete pathways for lipid biosynthesis are particularly common in
280 DPANN Cluster 2 representatives (incl. *N. equitans*) (**Figure 3, Supplementary Figure 62**)[10,13,14,71,72] and
281 the characterization of the *N. equitans - I. hospitalis* symbiotic system has confirmed the exchange of lipids
282 between symbiont and host[73]. Thus, while members of the Naiadarchaeales may synthesize their own
283 lipids, Undinarchaeales representatives may depend on an external source of archaeal or bacterial lipids

284 or intermediates in spite of the presence of the mevalonate pathway and their ability to synthesize
285 geranylgeranyl diphosphate (Supplementary Information). Similarly, the lack of several genes coding for
286 enzymes of the purine biosynthesis pathways in members of the Undinarchaeales but not
287 Naiadarchaeales, indicates that the former are also dependent on the external source of inosine
288 monophosphate (IMP) or other intermediates of the purine biosynthesis pathway (**Figures 2-3,**
289 **Supplementary Tables 7-8 and 9,** Supplementary Information).

290 Furthermore, all Undinarchaeota representatives lack genes encoding proteins involved in amino
291 acid and vitamin biosynthesis. Notably, and in agreement with several other potentially symbiotic DPANN
292 archaea[13,14], all Undinarchaeota representatives seem to contain a limited set of genes for transporters
293 such as amino acid transporter PotE and uncharacterized di/tri-carboxylate transporters (Supplementary
294 Information, **Figures 2-3**), suggesting that they are unable to acquire all essential building blocks directly
295 from the environment. In turn, members of the Undinarchaeota seem to depend on partner organisms to
296 provide compounds that cannot be synthesized or taken up from the environment using transporters. Key
297 differences among the biosynthetic capabilities of members of the Naiad- and Undinarchaeales, may
298 translate into varying substrate requirements and demands from potential host organisms.

299 *Cell-cell interactions.* Consistent with a host-dependent lifestyle, we detected several proteins
300 with domains known to be involved in cell-cell interactions and common among symbionts[13]. While
301 Undinarchaeota lack genes for ankyrin domain proteins and only encode a small number of beta
302 propeller/WD40 domain proteins, the proteome of members of the Naiadarchaeales comprises diverse
303 proteins with immunoglobulin domains, while Undinarchaeales encode Concanavalins/LamG domain
304 proteins (arCOG07813) (**Supplementary Tables 20-21**). Homology modeling and structure predictions
305 suggested that these proteins might encode potential cell adhesion proteins (**Supplementary Tables 22-**
306 **23**) and in turn may be involved in attachment or biofilm formation in Undinarchaeota. Notably, the
307 complete absence of LamG domain proteins in the Naiadarchaeales representatives indicates that
308 members of the two Undinarchaeota orders rely on different mechanisms mediating potential symbiont-
309 host interactions.

310 *Gene repertoires and reductive genome evolution in DPANN*. The presence and absence patterns
311 of genes involved in core metabolic pathways of Undinarchaeota MAGs shows similar trends as seen in
312 DPANN Cluster 2 archaea further supporting the sisterhood of this clade (**Figure 4, Supplementary Tables**
313 **7-9,12**). For instance, most DPANN Cluster 2 archaea lack genes involved in core metabolic pathways, such
314 as the electron transport chain, carbon fixation other than the RuBisCO gene, as well as transport and
315 motility genes (**Figure 3**)[10,13–16,23,25,39,74]. While Undinarchaeota seem to have more complete pathways
316 than many of the DPANN Cluster 2 representatives, they appear metabolically less flexible than several
317 members of DPANN Cluster 1 (**Figure 3**)[30,31,75,76]. For instance, members of the DPANN Cluster 1 have more
318 complete nucleoside and lipid biosynthesis pathways and include free-living organisms. In particular,
319 representatives of the Altiarchaeota have been suggested to comprise autotrophic archaea that may use
320 the Wood-Ljungdahl pathway for carbon fixation[24,25,30] and while this lineage includes symbionts, these
321 do not seem to be obligate[77,78]. In fact, Altiarchaeota have recently been found to include members that
322 likely serve as hosts for Huberarchaeota belonging to DPANN Cluster 2[25]. Furthermore, at least some
323 members of the Diapherotrites have been suggested to be capable of a fermentative free-living lifestyle[76].
324 However, in spite of overall gene repertoire patterns being consistent with results from our phylogenetic
325 analyses, there is a large variation in gene content and extent of genome reduction within DPANN

326 lineages[13]. Thus, our analyses further support the notion that while reductive genome evolution may have
327 characterized the evolution of Undinarchaeota and DPANN Cluster 2 archaea already at the time of their
328 divergence, the extent of streamlining varies widely and seems to have occurred in parallel in different
329 lineages[13].
330
331 **Insights into interaction partners of Undinarchaeota**
332 Genomic analyses of the first members of the Nanoarchaeota[39] as well as our marker protein
333 analyses have indicated that DPANN symbionts may have exchanged genes with their hosts. Furthermore,
334 co-occurrence patterns have recently allowed to pinpoint Altiarchaeota as host for the
335 Huberarchaeota[24,25]. Thus, to shed light onto potential interaction partners of the Naiad- and
336 Undinarchaeales, respectively, we have inferred routes of horizontal gene transfer and generated
337 proportionality networks.
338 In particular, we reconstructed phylogenies of proteins present in at least three Undinarchaeota
339 genomes (520 genes total) and analyzed sisterhood-relationships among taxonomically distinct lineages
340 including a reference set of 364 archaeal, 3020 bacterial and 100 eukaryotic genomes (**Figure 4,**
341 **Supplementary Tables 16-17,** Methods**,** Supplementary Information). Using this approach, we were able
342 to successfully detect signals of HGT among known host-symbiont pairs. For instance, our analysis
343 indicates that Nanoarchaeota and Huberarchaeota have exchanged 11% and 16% of the analyzed proteins
344 with their respective hosts belonging to the Crenarchaeota and Altiarchaeota, respectively. Furthermore,
345 our phylogenies suggest that Nanohaloarchaeota and Halobacteria shared a large amount of analyzed
346 proteins horizontally (12.4% and 7%) (**Figure 4**), which is in agreement with our core gene analyses
347 (**Supplementary Tables 4-5**). However, some of the sisterhood relationships could also be due to
348 compositional biases as a result of protein sequence adaptation to high salinity environments or
349 phylogenetic artifacts. Notably, Undinarchaeota does not show a dominant fraction of genes shared with
350 a specific lineage, i.e. most proteins seem to cluster with taxonomically closely related DPANN lineages
351 (**Figure 4**) or in some cases with potentially deeply branching Euryarchaeota such as
352 Hydrothermarchaeota or group 1 methanogens (**Supplementary Tables 4,16,17**). The few
353 Undinarchaeota genes that may have been shared with distantly related taxa encoded proteins that
354 grouped for instance with Bathyarchaeota and Thermoplasmata (i.e. including Poseidoniales and
355 Pontarchaea, or MG-II and -III) (Supplementary Information, **Supplementary Tables 4 and 16**). For
356 instance, the manual inspection of respective trees revealed that certain Undinarchaeota, in particular
357 marine Undinarchaeales, may have exchanged core genes with members of the Pontarchaea, including a
358 gene encoding ribosomal proteins S19 (arCOG04099, TIGR01025), respectively (**Supplementary Table 4**).
359 Yet, due to the small fraction of putative HGTs with any of these non-DPANN lineages relative to the total
360 proteome of Undinarchaeota, it remains to be assessed whether these patterns are genuine or result from
361 phylogenetic artifacts, lack of partner organisms in current databases or Undinarchaeota forming less
362 intimate interactions than DPANN Cluster 2 archaea.
363 Finally, we used a read-based co-occurrence analysis to assess whether MAGs of Undinarchaeota
364 are proportional to other archaeal and bacterial genomes[79] (see Methods for details). Due to the low
365 number of available samples for our inferences of co-proportionality, this analysis did not detect any
366 significant co-occurrence patterns for members of the Naiadarchaeales. However, it did indicate that

367 marine Undinarchaeales may co-vary with three genomes of the Chloroflexi, all belonging to the order
368 Dehalococcoidales (**Supplementary Figure 63**, Supplementary Information).
369 In turn, further analyses, such as fluorescence *in situ* hybridization, will be needed to identify the
370 organisms engaging in symbiotic interactions with Undinarchaeota. For instance, it will be important to
371 determine their host-specificity and test whether certain members of marine Undinarchaeales indeed
372 interact with members of the Chloroflexi or Pontarchaea. Together with previous findings[80], our results
373 suggest that certain DPANN symbionts could have non-archaeal partners highlighting the importance of
374 taking into account total community composition when inferring potential co-occurrences between
375 DPANN and other organismal groups.
376

377 Conclusions

378 We provided an updated view on the evolution of DPANN archaea by investigating the
379 phylogenetic placement and metabolic potential of the Undinarchaeota, a previously uncharacterized
380 archaeal lineage whose members have small genomes and limited metabolic gene repertoires indicative
381 of various auxotrophies. Its members, classified into the two order-level lineages Undinarchaeales and
382 Naiadarchaeales, may lead a symbiotic lifestyle and depend on (a) partner organism(s) for growth and
383 survival similar to other members of the various DPANN representatives[10,13,14]. In addition to insights into
384 the biology of members of the Undinarchaeota, their genomes contributed valuable data to address the
385 longstanding debate about whether DPANN indeed form a monophyletic clade or instead represent an
386 artifactual assemblage of phylogenetically disparate lineages[11,12,14,26–31,81,82]. In our analyses, which were
387 based on a broader taxon sampling, we not only attempted to account for the effect of compositional
388 biases but also developed a new method for detecting potential HGTs of marker proteins. Our results,
389 based on markers least effected by HGT, consistently recovered clan-hood of all DPANN lineages, such
390 that DPANN monophyly (i.e. monophyly of DPANN Cluster 1, Undinarchaeota and DPANN Cluster 2) solely
391 depends on the placement of the root. Notably, in analyses based on phylogenetic markers that had
392 indications for extensive inter-lineage HGT, Nanoarchaeota and Nanohaloarchaeota group with their
393 respective hosts the TACK-archaea and Halobacteria, respectively. This finding indicates that the previous
394 clading of certain DPANN lineages with Euryarchaeota[28,81] might to a certain degree be a result of
395 conflicting signals among marker proteins concatenated into one supermatrix. Finally, our analyses
396 robustly excluded the root from a clade consisting of Euryarchaeota, TACK and Asgard lineages,
397 strengthening the hypothesis that some or all of the DPANN superphylum diverged early from the
398 archaeal tree[27]. In turn, further exploration of DPANN promises to shed light on their roles in
399 biogeochemical cycles and food webs as well as the early evolution of cellular life and symbiosis.
400

401 Species description

402
403 *Description of Candidatus* Undinarchaeum (Un.din.ar.chae'um. L. n. *Undina* female water spirit or nymph
404 (from L. fem. n. *unda* water, wave); N.L. neut. n. *archaeum* (from Gr. adj. *archaios* ancient) archaeon; N.L.

405 neut. n. *Undinarchaeum* an archaeon of water origin). *Candidatus* Undinarchaeum marinum (ma.ri'num.
406 L. neut. adj. *marinum* of the sea, marine)

407 *Description of Candidatus* Undinarchaeum marinum (ma.ri'num. L. neut. adj. *marinum* of the sea, marine).
408 Type material is the genome designated as SRR2090159.bin1129 representing *Candidatus*
409 Undinarchaeum marinum.

410 *Description of Candidatus* Naiadarchaeum (Na.iad.ar.cha'eum. L. fem. n. *Naias*, *-adis* a water-nymph of
411 springs and streams, Naiad from Greek mythology; N.L. neut. n. *archaeum* (from Gr. adj. *archaios* ancient)
412 archaeon; N.L. neut. n. *Naiadarchaeum* an archaeon from the freshwater).

413 *Description of Candidatus* Naiadarchaeum limnaeum (lim.nae'um. N. L. neut. adj. *limnaeum* (from Gr. adj.
414 *limnaios* from the marsh, lake) living in the freshwater). Type material is the genome designated as
415 SRR4028224.bin17 representing *Candidatus* Naiadarchaeum limnaeum.

416 Based on these genera, we further propose the families *Candidatus* Undinarchaeaceae fam. nov. and
417 *Candidatus* Naiadarchaeaceae fam. nov., the orders *Candidatus* Undinarchaeales ord. nov. and
418 *Candidatus* Naiadarchaeales ord. nov., the class *Candidatus Undinarchaeia* class nov., and the phylum
419 *Candidatus* Undinarchaeota phylum nov.
420

421 Captions for Figures and Tables

422

423 **Table 1** | **Genome characteristics of Undinarchaeota MAGs**. General genome statistics, including genome
424 size, GC content, contig number and other quality characteristics (presence of 16S, 23S and 5S rRNA
425 genes). Additionally, the degree of genome completeness and contamination was estimated using
426 CheckM. The CheckM results were investigated for marker genes commonly absent in DPANN archaea
427 (Supplementary Information) and CheckM was re-run excluding seven marker proteins. The results of this
428 analysis are shown in brackets.
429

430 **Figure 1** | **Phylogenetic placement of Undinarchaeota**. (a) Maximum likelihood phylogenetic analysis
431 (LG+C60+F+R model) based on an alignment generated with the 50% top ranked marker proteins (n=56)
432 and 364 taxa set. For this alignment 10% of the most heterogeneous sites were removed using chi2
433 pruning. The full tree is shown in **Supplementary Figure 17**. (b) Bayesian phylogenetic tree (CAT+GTR
434 model) of an alignment generated with the 25% top ranked marker proteins (n=28) and 127 taxa set. For
435 this alignment 40% of the most heterogeneous sites were removed using chi2 pruning. The full tree is
436 shown in **Supplementary Figure 8**. Euryarchaeota 1 includes all Euryarchaeota with the exception of
437 Theionarchaea, Thermococci, Persephonarchaea and Hadesarchaea, which are clustered in
438 Euryarchaeota 2. Scale bar: Average number of substitutions per site. (c-f) Possible positions of the
439 archaeal root inferred using bacteria as an outgroup (c) or using the non-reversible model in IQ-TREE 2 (d-
440 f). All of these methods recover a clade of Undinarchaeota and Cluster 2 DPANN, consistent with
441 synapomorphies including a fused DNA primase and a reduced exosome that lacks Csl4.

Figure 2 | Metabolic characteristics of Undinarchaeota projected on key pathways. Full circles: Gene of interest is present in all or more than 50% of genomes. Half circles: Gene of interest is present in less than 50% but found in at least one Undinarchaeota MAG. Open circle: Gene is absent in all Undinarchaeota MAGs. Dark green: MAGs belonging to the marine Undinarchaeales. Light green: MAGs belonging to the aquifer Naiadarchaeales. **deo*A was only present in one Naiadarchaeales MAG and genes encoding RuBisCO were only found in two out of four Naiadarchaeales MAGs and it remains to be determined whether this is due to genome incompleteness or a sign of genome streamlining. A detailed list of genes encoded by Undinarchaeota can be found in **Supplementary Tables 7-9**.

Figure 3 | Occurrence of key metabolic proteins across major archaeal lineages. Protein occurrence was calculated by detecting key proteins of interest across 364 archaeal genomes and calculating the occurrence in percent across the total number of genomes included in each phylogenetic cluster based on a presence/absence table. Number in brackets: number of genomes included in each individual phylogenetic cluster. CF = Carbon fixation. FD = Fatty acid degradation. A table listing gene occurrences in archaeal lineages can be found in **Supplementary Table 9** and a list of metabolic genes shown in this plot can be found in **Supplementary Table 19**.

Figure 4 | **Potential HGTs of core proteins of Undinarchaeota across archaeal lineages**. The plot is based on phylogenetic analyses of 520 core proteins (shared across at least three MAGs of the Undinarchaeota), which included a representative set of archaeal, bacterial and eukaryotic genomes (n=3482 taxa). In particular, this plot depicts sisterhood-relationships observed in these phylogenies for all major archaeal lineages including the Undinarchaeota (see **Supplementary Table 18** for the full list of genomes used and **Supplementary Table 16-17** for the accompanying data for the HGT analysis). See custom scripts and Methods for more details.

Methods

Genome recovery and reconstructions

Reconstructing MAGs of Undinarchaeota

We mined the Sequence Read Archive (SRA) for public metagenomes using SingleM (https://github.com/wwood/singlem). Thereby, we found 37 metagenomes containing reads assigned to Undinarchaeota (**Supplementary Table 1**). Genomes from these 37 metagenomes were recovered by assembly with megahit (v1.1.3)[83], mapping raw reads from each sample to its corresponding assembly using BamM (v1.7.3) (https://github.com/Ecogenomics/BamM) using BWA 'mem' (v0.7.15)[84] with default parameters. Binning was carried out with MetaBAT (v2.11.1)[85] using default parameters and allowed the reconstruction of six MAGs. The quality of these six as well as the six previously published Undinarchaeota MAGs was assessed using CheckM (v1.0.7)[86]. Additionally, the CheckM marker set was screened for markers that were absent in all 12 Undinarchaeota MAGs. Thereby, we identified 7 markers (PF01287,

482 PF01667, PF01912, PF01982, PF04127, TIGR00432 and TIGR01213) that were not only absent in
483 Undinarchaeota but often in other DPANN archaea (Supplementary Information). As the inclusion of these
484 markers might underestimate the completeness scores, we also ran CheckM excluding these markers.
485 Both results are summarized in **Table 1**.
486
487 Contamination Screening
488 Contigs from all 12 Undinarchaeota MAGs were manually investigated for signs of contamination
489 by looking for an abnormal GC-content (~10% difference in average GC-content) and/or taxonomic
490 composition. To determine the taxonomic composition, the protein files of each genome (see section
491 below) were searched against the NCBI-non-redundant (nr) database (downloaded in November 2018)
492 using DIAMOND v0.9.22.123 (settings: --more-sensitive --evalue 1e-10 --seq 100 --no-self-hits --taxonmap
493 prot.accession2taxid.gz)[87]. The best hit for each protein was selected based on the highest e-value and
494 bit-score. Subsequently, the obtained NCBI taxonomy identifier was merged with the taxonomic string
495 information provided by NCBI using a mapping file generated in January 2019 using ncbitax2lin
496 (https://github.com/zyxue/ncbitax2lin). Contigs with an "abnormal" taxonomic distribution (>90% of
497 proteins on a contig assigned to a non-archaeal or non-DPANN lineage with a percentage identity above
498 80%) were either removed or confirmed by phylogenetic analyses of single gene trees (see Supplementary
499 Information).
500 Notably, several Undinarchaeota MAGs appeared to encode a short genomic region similar to an
501 archaeal fosmid sequence deposited at NCBI and referred to as uncultured marine group I/III
502 euryarchaeote KM3_51_D01 (https://www.ncbi.nlm.nih.gov/nuccore/663520902). In particular, proteins
503 encoded in this region shared about 84% ANI to protein homologs found on this fosmid. To investigate
504 whether our MAGs may be contaminated by contigs of members of the MGII/III archaea
505 (Pontarchaea/Poseidoniales), we performed single protein trees of marker proteins located in this
506 genomic region and queried the ORFs located on fosmid KM3_51_D01 against NCBI-nr Importantly, our
507 results (i) suggested that this fosmid does not belong to the Pontarchaea/Poseidoniales archaea and
508 should be reclassified as "uncultured archaeon KM3" and (ii) verified, that respective genomic regions in
509 our MAGs are not contaminated. Please see Supplementary Information for further details.
510
511 **Phylogenetic analyses**

512 Generation of a backbone datasets for phylogenetic analyses

513 **Archaeal backbones**. To generate a representative archaeal reference set all archaeal genomes
514 were downloaded from NCBI (January 2019). Genomes with a completeness >40% and contamination
515 <25% (determined with CheckM lineage_wf v1.0.11)[86] were used for an initial phylogenetic analysis using
516 the PhyloSift marker set. In brief, homologs of 34 PhyloSift marker proteins were identified in each
517 genome using the PhyloSift v1.0.1 'find' mode (settings: --besthit)[48]. Subsequently, marker proteins were
518 individually aligned using MAFFT L-INS-i v7.407 (settings: --reorder)[88] and trimmed using BMGE v1.12
519 (settings: -m BLOSUM30 -h 0.55)[89]. The concatenated protein alignment was used to reconstruct a
520 phylogenetic tree using IQ-TREE v1.6.7 (settings: -m LG -nt AUTO -bb 1000 -alrt 1000)[50,58,59]. Based on this
521 tree, a sub-selection of 364 archaeal reference genomes was generated (comprising 352 reference
522 archaeal and 12 Undinarchaeota genomes, **Supplementary Table 18**), which covers the archaeal

523 phylogenetic diversity while still allows to perform computationally intensive phylogenetic analyses
524 needed to resolve the placement of DPANN in the tree of Archaea. Selected genomes preferentially
525 derived from type strains as well as from known hosts of DPANN archaea. Furthermore, representative
526 MAGs and SAGs were selected based on high completeness and low degree of contamination. Based on
527 an initial maximum likelihood analysis (IQ-TREE, C60+LG model) including these 364 species, *Zestosphaera*
528 *tikiterensis* NZ3 seems to represent a lineage of the order Sulfolobales rather than the Desulfurococcales[90]
529 with high statistical support (i.e. bootstrap of >97%, **Supplementary Figure 9**). Furthermore, the
530 placement of "Acidilobales" within the Desulfurococales was highly supported (i.e. bootstrap of 100%,
531 **Supplementary Figure 9**), which indicates that Acidilobaceae represents a family level lineage within the
532 Desulfurococcales rather than an order level lineage[91]. This also corresponds to the taxonomy of the
533 Genome Taxonomy Database (GTDB; https://gtdb.ecogenomic.org). We therefore assigned both
534 *Zestosphaera tikiterensis* NZ3 and Acidilobaceae to the Desulfurococcales in our analyses.
535 To create a smaller archaeal reference set suitable for Bayesian phylogenies, the 364 archaeal
536 genome set was further subsampled to only include 127 taxa. In particular, at least two members of all
537 major archaeal order-level lineages were selected based on phylogenetic distance, genome quality. For
538 MAGs that were only classified at phylum level (i.e. Woesearchaeota), we selected a representative set of
539 taxa based on the 364 species tree.
540 **Bacterial backbones**. To generate a bacterial backbone, we downloaded a list of available
541 genomes from NCBI in 2018 (ftp://ftp.ncbi.nlm.nih.gov/genomes/genbank/bacteria/). This list was parsed
542 to only include type strains or representative genomes. From this list we randomly selected a
543 representative strain per genus. In a second step, we selected 15-30 genomes from candidate phyla from
544 the unparsed list. This initial set was screened for completeness and contamination in CheckM[86] and
545 genomes with less than 50% completeness and more than 10% contamination were excluded. We
546 performed initial phylogenies using alignments generated by PhyloSift[48] using the PhyloSift search, align
547 and name algorithms to find marker proteins. Individual genes were aligned with MAFFT L-INS-i (settings:
548 --reorder)[88] and trimmed using BMGE (settings: -m BLOSUM30 -h 0.55)[89]. The concatenated protein
549 alignment was used to reconstruct a phylogenetic tree using IQ-TREE v1.6.7 (settings: -m LG -bb 1000 -
550 alrt 1000)[50]. The initial alignments were screened for long-branches and genomes that did not fall into the
551 expected position in the tree were removed from the taxa selection resulting in a set of 3020 bacterial
552 genomes.
553 **Eukaryotic backbones**. 98 eukaryotic genomes and largely complete transcriptomes were
554 selected so as to obtain even sampling across the known major lineages of eukaryotes. Where possible,
555 we selected free-living representatives of clades with a completely sequenced genome; alternatively, we
556 selected the most complete transcriptome from a free-living member of the group.

557 Selection of marker proteins for phylogenetic analyses

558 To accurately place Undinarchaeota in the archaeal tree of life, we identified suitable markers
559 among three different but overlapping marker proteins sets: (a) a set of herein identified potential single-
560 copy, near universal archaeal orthologues and the marker protein sets implemented in GTDB (b) and
561 PhyloSift (c).
562 (a) We inferred a set of markers by running the OMA standalone algorithm[92] on a set of 149
563 archaeal genomes chosen to represent known taxonomic diversity. We inferred single protein trees for

564 97 orthologues that were present in at least 75% of the genomes and manually inspected the resulting
565 trees to identify and remove 15 markers that had undergone gene transfer, resulting in a final set of 82
566 candidate single-copy orthologs.
567 (b) The GTDB marker set was downloaded February 2019 (release r86 downloaded from
568 https://gtdb.ecogenomic.org). This set was modified by combining the 122 archaeal GTDB marker set with
569 the complete TIGRFAM database. Therefore, the extra PFAMs defined in the GTDB marker set were added
570 to the TIGRFAM database (TIGRFAMs_15.0_HMM.LIB: downloaded Sept 2018) and the combined
571 database will be referred to as TIGRFAM_GTDB.
572 (c) The PhyloSift marker set[48] included all previously reported markers excluding genes for the
573 phenylalanine synthetase. These three marker sets were combined by adding the PhyloSift and OG marker
574 protein set to the TIGRFAM_GTDB database with the final database consisting of 151 non-redundant
575 protein families.

576 Assessment of the 151 marker set for suitability in concatenations

577 Homologs in the bacterial, eukaryotic and archaeal backbone datasets as well as in
578 Undinarchaeota MAGs were identified using hmmsearch v3.1b2 (settings: -E 1e-20)[93]. The output was
579 parsed to only include the best hit based on the e-value and bit-score. Afterwards, marker proteins were
580 individually aligned using MAFFT L-INS-i (settings: --reorder)[88] and trimmed using BMGE (settings: -t AA -
581 m BLOSUM30 -h 0.55)[89]. Subsequently, we inferred single protein phylogenies with IQ-tree (settings: -m
582 LG+G+F+R -bb 1000 -alrt 1000)[50] for each of these 151 marker protein families, including homologs
583 identified in the corresponding reference genomes (i.e. 364 archaea, 3020 bacteria and 98 eukaryotes
584 (see details above). Marker proteins in which archaea and eukaryotes were not monophyletic (i.e.
585 archaeal lineages were paraphyletic with some lineages emerging from within Bacteria), were excluded
586 from any further analysis (see also **Supplementary Tables 4-5**).
587 Next, we used a custom python script (count_sister_taxa.py;
588 https://github.com/Tancata/phylo/blob/master/count_sister_taxa.py) to rank each marker protein
589 phylogeny based on the extent to which it resolved monophyletic clades of well-established archaeal
590 phylum- or order-level lineages. In brief, the script counts for each tree, how many times a certain taxon
591 does not group with its expected taxonomic clade across all bootstrap trees, thus representing so-called
592 splits. Splits (which may arise through HGT or phylogenetic artifacts) are counted for each taxon across all
593 protein phylogenies and provide the basis for ranking the different markers according to their reliability.
594 Here, we counted both the total number of splits as well as the splits normalized to the total species count.
595 Note, monophyly was assessed on the level of following archaeal clades: Geothermarchaeota,
596 Halobacteria, Methanonatronarchaeales, Methanomicrobiales, Methanosarcinales, Methanocellales,
597 Methanophagales, Archaeoglobales, Thermoplasmatales, Acidiprofundales, Methanomassiliicoccales,
598 Poseidoniales, Thermoplasmata (not assigned at order level), Pontarchaea, Undinarchaeota,
599 Woesearchaeota, Pacearchaeota, NovelDPANN_1 (UAP1), Parvarchaeota, Nanohaloarchaeota,
600 Aenigmarchaeota, Diapherotrites, Huberarchaeota, Micrarchaeota, Altiarchaeota, Methanopyrales,
601 Methanobacteriales, Methanococcales, Desulfurococcales, Sulfolobales, Thermoproteales,
602 Marsarchaeota, Thermococcales, Theionarchaea, Methanofastidiosa, Hadesarchaea, Persephonarchaea,
603 Odinarchaeota, Verstraetearchaeota, Thorarchaeota, Lokiarchaeota, Heimdallarchaeota,
604 Bathyarchaeota, Thaumarchaeota, Korarchaeota, Aigarchaeota, Geoarchaeales, Hydrothermarchaeota

605 and Nanoarchaeota. The number of split phylogenetic clusters (in percentage) as well as the total number
606 of splits normalized by the total number of species within each tree was used as criteria to rank and define
607 the 25%, 50% and 75% top as well as 25% and 50% lowest ranking marker proteins (**Supplementary Tables**
608 **4-5**). Finally, the 50% top-ranking single protein trees were manually inspected for signs of contamination
609 or paralogues that were then manually removed from the marker protein sequences. After manual
610 cleaning, the marker proteins were aligned using MAFFT L-INS-i[88] and trimmed using BMGE[89] as described
611 above. The single proteins were concatenated using catfasta2phyml.pl
612 (https://github.com/nylander/catfasta2phyml). Note that all single protein phylogenies as well as the
613 individual protein files and alignments have been deposited in a Zenodo repository
614 (10.5281/zenodo.3672835).

615 Phylogenetic analyses for the species trees

616 To confirm the placement of Undinarchaeota several different phylogenetic trees were generated (all
617 trees are summarized in **Supplementary Table 6** and shown in full in **Supplementary Figures 6-56**):
618
619 **(I) Using different subsets of marker proteins for maximum-likelihood phylogenies**
620 The alignment for the concatenated 25%, 50% and 75% top as well as 25% and 50% lowest ranking
621 marker proteins were generated for the 364 as well as 127 taxa set and phylogenetic trees were generated
622 using IQ-TREE (v1.6.7, settings: -m LG+C60+F+R -bb 1000 -alrt 1000)[50].
623 **(II) Stationary trimming for maximum-likelihood phylogenies**
624 The concatenated alignment for the 50% top ranking marker proteins was aligned with MAFFT L-
625 INS-i[88] and trimmed with BMGE[89] using stationary trimming (options: -s FAST -h 0:1 -g 1) to remove
626 compositional heterogenous sites from both the 127 and 364 taxa set. Trees were generated using IQ-
627 TREE[50](settings: -m LG+C60+F+R -bb 1000 -alrt 1000).
628 **(III) Data recoding for maximum-likelihood phylogenies**
629 The concatenated alignment for the 50% top ranking marker proteins (alignment: MAFFT L-INS-
630 i[4], trimming: BMGE[89]) was re-coded into 4 character-states (SR4 re-coding[94]; i.e. data simplification from
631 20 to four character states) to reduce compositional heterogeneity both for the 127 and 364 taxa set using
632 a custom script (Recode_aa.py). The states used were the following: A,G,N,P,S,T = A; C,H,W,Y = C;
633 D,E,K,Q,R = G and F,I,L,M,V = T. Phylogenetic trees were generated using IQ-TREE (settings: -m C60SR4 -
634 bb 1000 -alrt 1000).
635 **(IV) Removing fast-evolving sites for maximum-likelihood phylogenies**
636 SlowFaster[95] was used on the concatenated alignment for the 50% top ranking marker proteins
637 (alignment: MAFFT L-INS-i[88], trimming: BMGE[89]; settings see above) to remove fast-evolving sites both
638 from the 127 and 364 taxa set. Sites were removed in a stepwise manner removing 10%, 20%, 30% and
639 40% of the fastest evolving sites. Phylogenetic trees were generated using IQ-TREE[50] (settings: -m
640 LG+C60+F+R -bb 1000 -alrt 1000).
641 **(V) Removing heterogenous sites for maximum-likelihood phylogenies**
642 Alignment_pruner.pl (https://github.com/novigit/davinciCode/blob/master/perl) was used to
643 remove heterogenous sites in a stepwise manner from the concatenated alignment for the 50% top
644 ranking marker proteins (alignment: MAFFT L-INS-i[88], trimming: BMGE[89]; settings see above) both from
645 the 127 and 364 taxa set. Sites were removed in a stepwise manner removing 10%, 20%, 30% and 40% of

646 the most heterogeneous sites and the trees were generated using IQ-TREE[50] (settings: -m LG+C60+F+R -
647 bb 1000 -alrt 1000).
648 **(VI) Using published marker gene sets for maximum-likelihood phylogenies**
649 Several alternative marker sets were used to confirm the tree topologies. These include the
650 PhyloSift marker set[48] using the default alignment with hmmalign[96] or MAFFT L-INS-i[88], the 122 archaeal
651 GTDB marker set[49] using FastTree v2.1.10[97](settings: WAG, LG) or IQ-TREE[50] (settings: LG+C60+F+R), the
652 RP14 marker set[10] and the universal 48 marker set[6]. Please note that the PhyloSift[48], 122 GTDB marker
653 gene set[49] and RP14 marker protein[10] set were subjected to phylogenetic analyses before defining the 364
654 taxa set and include slightly less taxa (356).
655 **(VII) Using different subsets of marker proteins for Bayesian phylogenies**
656 The concatenated alignment for the 25% and 50% top ranking marker proteins (alignment: MAFFT
657 L-INS-i[88], trimming: BMGE[89] and the 127 taxa set were used for Bayesian inferences using PhyloBayes-MPI
658 v1.8[51] (settings: -cat -gtr -x 10 -1 -dgam 4). In particular, for each marker protein family, four parallel chains
659 were run until convergence was reached, unless stated otherwise (maxdiff < 0.3; settings: bpcomp -x
660 25%_burnin chain1 chain2 chain3 chain4). Additionally, we checked for the minimum effective size using
661 tracecomp (minimum effective size > 50; settings: -x 25%_burnin chain1 chain2 chain3 chain4).
662 Subsequently, readpb_mpi of the pb_mpi package was used for posterior predictive testing (settings: --
663 allpred).
664 **(VIII) Rooting maximum-likelihood phylogenetic trees using non-reversible models**
665 To root our phylogenetic trees, we analyzed the concatenated alignment based on the 50% top
666 ranking marker proteins using a single partition model and a multiple partition non-reversible model.
667 These analyses were performed on the 127 and 364 taxa set using the full alignments and the recoded
668 alignments in which 20% or 40% of the most heterogeneous sites were removed. Trees were generated
669 with an updated version of IQ-TREE v2[57] (while all previously mentioned phylogenies were generated with
670 IQ-TREE v1)[50]. The single partition models were run with the following settings: -mset LG -bb 1000 -alrt
671 1000 -m MFP+MERGE, followed by --model-joint NONREV --min-freq 0.001 -nparam 10 -optfromgiven -
672 bb 1000 -alrt 1000. The multiple partition model was run with these settings: -model-joint NONREV --min-
673 freq 0.001 -nparam 10 -optfromgiven -bb 1000 -alrt 1000. Additionally, we used minimal ancestor
674 deviation (MAD) rooting to determine the root position[98].
675 **(IX) Rooting maximum-likelihood phylogenetic trees using bacteria as an outgroup**
676 To root our phylogenetic trees with bacteria as an outgroup we added 88 bacterial genomes to
677 our 127 archaeal taxa selection. These 88 bacterial genomes were selected from the bacterial backbone
678 tree by covering a broad diversity and including at least one to three genomes per phylum. However, to
679 minimize LBA artifacts, we did not select members of the CPR[99] as well as other symbionts or
680 thermophiles, which often emerge on long branches in phylogenetic trees[100,101]. Next, we identified
681 homologs of the universal 48 markers[6] in each genome, individually aligned proteins using MAFFT L-INS-
682 i[88] (settings: --reorder) and trimmed using BMGE (settings: -t AA -m BLOSUM30 -h 0.55)[89]. Single proteins
683 were concatenated using catfasta2phyml.pl (https://github.com/nylander/catfasta2phyml) and a
684 phylogenetic tree was generated using IQ-TREE (settings: -m LG+C60+F+R -bb 1000 -alrt 1000).
685

686 **Phylogenetic analyses of the core Undinarchaeota protein set**

687 A set of 520 proteins for Undinarchaeota were selected based on arCOGs detected in at least
688 three or more Undinarchaeota genomes with an e-value greater than 1e-20 (see below). Next, these 520
689 arCOGs were queried against a protein database of 364 archaeal, 3020 bacterial and 98 eukaryotic
690 genomes using PSI-BLAST (settings: -evalue 1e-20 -show_gis -outfmt 6 -max_target_seqs 1000 -dbsize
691 100000000 -comp_based_stats F -seg no) against the arCOG database (version from 2014)[102]. Protein
692 alignments were generated for each individual protein family using MAFFT L-INS-i[88] (protein alignments
693 with <1000, settings: --reorder) or MAFFT (alignments with >1000 sequences, settings: --reorder).
694 Afterwards, all alignments were trimmed using BMGE[89] (settings: -t AA -m BLOSUM30 -h 0.55).
695 Phylogenetic trees were generated using IQ-TREE[50] (settings: -m LG+G -wbtl -bb 1000 -bnni). To search for
696 HGT events, trees were analyzed using the script count_sister_taxa.py
697 (https://github.com/Tancata/phylo/blob/master/count_sister_taxa.py), which allows to determine the
698 closest sister lineage of any taxon of interest in an unrooted phylogeny, i.e. the sister lineage is defined as
699 the lineage in the smallest sister group while all other taxa are the outgroup. Cases in which homologs of
700 Undinarchaeota formed a sister lineage to non-DPANN, were visually confirmed and all hits for
701 Undinarchaeota are listed in **Supplementary Tables 16-17**.
702

703 **Phylogenetic analyses of 16S and 23S rRNA genes**

704 16S and 23S rRNA gene sequences were identified in all archaeal genomes using Barrnap v0.9[103]
705 (settings: --kingdom arc --evalue 1e-20; https://github.com/tseemann/barrnap). Partial sequences and
706 sequences shorter than 400 bp were removed prior to extracting the sequences using bedtools v2.26.0[104].
707 Subsequently, sequences were individually aligned using MAFFT L-INS-i[88] and trimmed using
708 TrimAL[105](v1.2rev59, -automated1 setting) or BMGE[89] (settings: -t DNA -m DNAPAM100:2 -h 0.55) and
709 concatenated (https://github.com/nylander/catfasta2phyml). 16S and 23S rRNA gene homologs located
710 on the same contig were concatenated whenever more than one copy of the 16S or 23S rRNA gene was
711 encoded by a genome. Alignment_pruner.pl (https://github.com/novigit/davinciCode/blob/master/perl)
712 was used to remove the 10% most heterogenous sites from the alignment. After running an initial tree
713 with all 16S-23S rRNA gene sequences using IQ-TREE, we confirmed that MAGs with multiple copies
714 clustered together and removed all but one representative copy for the following tree. Additionally, we
715 removed 16S and 23S rRNA homologs of the genome-reduced Huberarchaeota to avoid potential long-
716 branch attraction artifacts. A phylogenetic tree was generated with IQ-TREE for the full-length alignment
717 trimmed with TrimAL[105] (setting: -automated1), BMGE[89] (settings: -t DNA -m DNAPAM100:2 -h 0.55) as
718 well as the 10% pruned TrimAL alignment (IQ-TREE; settings: -m GTR+G -bb 1000 -alrt 1000)[50]. The trees
719 are provided in **Supplementary Figures 3-5**.
720

721 **Phylogenetic analyses of the RuBisCO gene**

722 RuBisCO protein sequences were identified by their arCOG ID (arCOG04443), which was identified
723 in all Undinarchaeota as described in section 'Gene calling and annotation'. Subsequently, we extracted
724 the sequences for the RuBisCO protein from Undinarchaeota and combined them with an unmasked
725 alignment generated in a previous study[67] using mafft_align[88] with the --add option. The alignment was
726 trimmed using BMGE (-g 0.5 -b 1 -m BLOSUM30 -h 0.55)[89] and a tree generated using IQ-TREE (-m LG+G -
727 wbtl -bb 1000 -bnni). The conservation of the catalytic site was compared in reference to *Synechococcus*

728 *elongatus* PCC_6301 as described previously[67]. The tree is provided in **Supplementary Figure 59**. The logo
729 for the catalytic site was generated with logomaker v0.8 in python v2.7.15[106].
730
731 **Phylogenetic analyses of the archaeal DNA primase**
732 To compare the phylogenetic history of the canonical and the fused PriL and PriS subunits of the
733 primase we extracted arCOGs corresponding to the two subunits (arCOG04110 for PriS and arCOG03013
734 for PriL, respectively) from the 364 reference archaeal genomes. To determine the conserved domains for
735 PriS and PriL in both the fused and canonical proteins we uploaded the sequences to the Conserved
736 Domain Search Service (CD-Search) web-based tool using default settings (**Supplementary Table 11**). The
737 start and end positions provided by CD-Search were used to split the fused version of the primase into
738 "unfused" PriS and PriL subunits using bedtools getfasta. The sequences for the canonical PriS and PriL as
739 well as split PriS and PriL were combined and aligned using MAFFT L-INS-i[88](option --reorder) and trimmed
740 using TrimAL[105] (-gappyout). A phylogenetic tree was generated with IQ-TREE (-m LG+F+C10 -bb 1000 -alrt
741 1000)[50]. The tree is provided in **Supplementary Figure 57**.
742
743 **Gene calling and annotation**
744 We annotated the 12 MAGs of Undinarchaeota (six from this study) as well as our set of 352
745 archaeal reference genomes. Gene calling was performed using Prokka[107] (v1.14, settings: --kingdom
746 Archaea --addgenes --increment 10 --compliant --centre UU --norrna --notrna). For further functional
747 annotation, the generated protein files were compared against several databases, including the arCOGs
748 (version from 2014)[102], the KO profiles from the KEGG Automatic Annotation Server[108] (KAAS; downloaded
749 April 2019), the Pfam database[109] (Release 31.0), the TIGRFAM database[110] (Release 15.0), the
750 Carbohydrate-Active enZymes (CAZy) database[111] (downloaded from dbCAN2 in September 2019), the
751 MEROPs database[112] (Release 12.0), the Transporter Classification Database[113] (TCDB; downloaded in
752 November 2018), the hydrogenase database[114] (HydDB; downloaded in November 2018) and NCBI_nr
753 (downloaded in November 2018). Additionally, all proteins were scanned for protein domains using
754 InterProScan (v5.29-68.0; settings: --iprlookup --goterms)[115].
755 Individual database searches were conducted as described in the following section. ArCOGs were
756 assigned using PSI-BLAST v2.7.1+ (settings: -evalue 1e-4 -show_gis -outfmt 6 -max_target_seqs 1000 -
757 dbsize 100000000 -comp_based_stats F -seg no)[116]. KOs as well as PFAMs, TIGRFAMs and CAZymes were
758 identified in all archaeal genomes using hmmsearch v3.1b2[96] (settings: -E 1e-4). The Merops database was
759 searched using BLASTp v2.7.1 (settings: -outfmt 6, -evalue 1e-20). For all database searches the best hit
760 for each protein was selected based on the highest e-value and bitscore and all results are summarized
761 for Undinarchaeota in **Supplementary Table 7**. For InterProScan we report multiple hits corresponding to
762 the individual domains of a protein using a custom script (parse_IPRdomains_vs2_GO_2.py). Additionally,
763 tRNA genes were identified from contigs of Undinarchaeota and all archaeal reference genomes using
764 tRNAscan-SE v2.0[117] and the results are summarized in **Supplementary Table 10.**
765 Proteins potentially involved in cell-cell interactions (**Supplementary Table 20**, some of which
766 were reported in Castelle et al., 2018[13]) were separately screened with HHpred[118] and Phyre2[119]. HHpred
767 was run on a local server by first running hhblits the uniclust30_2018_08 database (settings: -E 1E-03, -
768 oa3m). The alignment file in a3m format was used as an input in hhsearch against the pdb70 database
769 (settings: -p 20 -Z 250 -loc -z 1 -b 1 -B 250 -ssm 2 -sc 1 -seq 1 -dbstrlen 10000 -norealign -maxres 32000 -

770 contxt context_data.crf -blasttab). Protein homology was investigated using Phyre2 by using the batch
771 upload function of the web-version.
772
773 **Metabolic comparisons**
774 Results from the gene calling and annotation described above were used as basis for comparative
775 genome analyses and metabolic comparisons. For simplicity we reported gene presence/absence patterns
776 on class level whenever possible, while DPANN and most taxa without cultured representatives were
777 defined at the phylum level. First, the occurrence of each individual gene found across each
778 MAG/reference genome was counted in R (v3.5.0). This count table provided the basis for summary tables
779 generated using the ddply function of the plyr package (v 1.8.4). The results of these analyses are
780 summarized in **Supplementary Tables 9 and 12**. To plot the heatmap shown in **Figure 3**, the count table
781 was first transferred to a presence/absence matrix and the ddply function was used to summarize the
782 counts across each phylogenetic cluster. The data was visualized as a heatmap using the ggplot function
783 with geom_tile and facet_wrap of the ggplot2 package v3.0.0. A table summarizing the gene IDs used can
784 be found in **Supplementary Table 19**. The heatmap was manually merged with the collapsed tree in
785 Inkscape v0.91.
786
787 **Average amino acid identity**
788 The average amino acid identity (AAI) across all archaeal reference genomes and the 12
789 Undinarchaeota MAGs was calculated using comparem v0.0.23 (settings: aai_wf)[120]. The output was
790 summarized in R (v3.5.0) using the packages reshape2 (v1.4.3), plyr (v1.8.4) and dplyr (v0.7.6) generating
791 the **Supplementary Table 3** and ggplot2 (v3.0.0) and ggpubr (v0.2) to plot the data.
792
793 **Undinarchaeota co-occurrence analysis**
794 37 SRA metagenomes (**Supplementary Table 1**) containing reads assigned to Undinarchaeota
795 were pseudo-aligned to a genome dataset consisting of 6,890 GTDB r89 archaeal and bacterial genus-
796 dereplicated genomes (GTDB; https://gtdb.ecogenomic.org) and 12 Undinarchaeota MAGs using the
797 software Kallisto v.0.44.0 with the default k-mer size (31 bp)[121]. To reduce the number of false positive
798 genomes, the pseudo-alignment results were subjected to three filtering criteria published previously[121].
799 The subset of genomes that fulfilled the three criteria was used to create a reference database for read
800 mapping of the 37 SRA metagenomes via bamM using default parameters
801 (https://github.com/Ecogenomics/BamM). Relative abundances (Ar) were normalized based on the total
802 read counts, i.e. the maximum number of reads of all metagenomes (Nm) divided by the sample read
803 count (Ns), multiplied by number of reads of that particular sample that mapped to the genome (r), and
804 the average read length (l), divided by the genome size (g) ($Ar=Nm/Ns * (r*l/g)$)[25,79]. Proportionality was
805 analyzed using the R package propR[79] based on normalized relative abundances, followed by the centered
806 log-ratio transformation. Only metagenomes containing maximum UAP2 normalized relative abundance
807 above 1.0 were included in this step (that resulted in 27 metagenomes involved in calculating
808 proportionality). Finally, genomes that were proportional ($\rho \geq 0.9$) to more than three Undinarchaeota
809 MAG were identified as Undinarchaeota co-correlated.

Data and Code availability

The datasets analyzed during the current study are available in the NCBI repository at https://www.ncbi.nlm.nih.gov/ and the accession numbers can be found in Supplementary Table 1. New MAGs generated from the current study have been deposited at NCBI GenBank and can be accessed under BioProject **PRJNA609027** as well as via our repository at Zenodo. Furthermore, additional supplementary files including: (a) genome files including the contigs and protein files for all 12 Udinarcheota MAGs as well as the 352 reference genomes, (b) phylogenies for the species and single gene tree analyses including protein files, alignments and treefiles (Supplementary Figures 6-56) and (c) workflows for the annotations and phylogenies as well as custom python and R-scripts (to analyze tree files), perl code (to parse data) and R codes (to parse the data and generate figures) have been deposited at Zenodo with the **doi: 10.5281/zenodo.3672835**.

Acknowledgements

This work was supported by a grant of the Swedish Research Council (VR starting grant 2016-03559 to AS), the NWO-I foundation of the Netherlands Organization for Scientific Research (WISE fellowship to AS), and an Australian Research Council (ARC) Future Fellowship (FT170100213, awarded to CR). TW was supported by a Royal Society University Research Fellowship. BW was supported by the Australian Research Council Discovery Early Career Research Awards #DE160100248.

We want to thank Damien de Vienne for helpful discussion regarding testing of protein tree congruency as well as Celine Petitjean for sharing genomic and transcriptomic data of a selection of representative eukaryotes. We are also grateful to those that made their metagenomic datasets publicly accessible, including Pierre Offre for the MOCA dataset, Jill Banfield for the aquifer metagenomes, Peer Bork for the Indian Ocean metagenomes and Francisco Rodriguez-Valera for the Mediterranean metagenomes.

References

1. Woese, C. R. & Fox, G. E. Phylogenetic structure of the prokaryotic domain: The primary kingdoms. *PNAS* **74**, 5088–5090 (1977).
2. Williams, T. A., Foster, P. G., Cox, C. J. & Embley, T. M. An archaeal origin of eukaryotes supports only two primary domains of life. *Nature* **504**, 231–236 (2013).
3. Williams, T. A., Cox, C. J., Foster, P. G., Szöllősi, G. J. & Embley, T. M. Phylogenomics provides robust support for a two-domains tree of life. *Nat Ecol Evol* **4**, 138–147 (2020).
4. Spang, A. *et al.* Complex archaea that bridge the gap between prokaryotes and eukaryotes. *Nature* **521**, 173–179 (2015).

845 5. Eme, L., Spang, A., Lombard, J., Stairs, C. W. & Ettema, T. J. G. Archaea and the origin of eukaryotes. *Nature*
846 *Reviews Microbiology* **15**, nrmicro.2017.133 (2017).
847 6. Zaremba-Niedzwiedzka, K. *et al.* Asgard archaea illuminate the origin of eukaryotic cellular complexity.
848 *Nature* **541**, 353–358 (2017).
849 7. Hug, L. A. *et al.* A new view of the tree of life. *Nature Microbiology* **1**, 16048 (2016).
850 8. Adam, P. S., Borrel, G., Brochier-Armanet, C. & Gribaldo, S. The growing tree of Archaea: new perspectives
851 on their diversity, evolution and ecology. *The ISME Journal* **11**, 2407–2425 (2017).
852 9. Spang, A., Caceres, E. F. & Ettema, T. J. G. Genomic exploration of the diversity, ecology, and evolution of the
853 archaeal domain of life. *Science* **357**, eaaf3883 (2017).
854 10. Castelle, C. J. & Banfield, J. F. Major new microbial groups expand diversity and alter our understanding of
855 the tree of life. *Cell* **172**, 1181–1197 (2018).
856 11. Rinke, C. *et al.* Insights into the phylogeny and coding potential of microbial dark matter. *Nature* **499**, 431–
857 437 (2013).
858 12. Castelle, C. J. *et al.* Genomic expansion of domain archaea highlights roles for organisms from new phyla in
859 anaerobic carbon cycling. *Current Biology* **25**, 690–701 (2015).
860 13. Castelle, C. J. *et al.* Biosynthetic capacity, metabolic variety and unusual biology in the CPR and DPANN
861 radiations. *Nature Reviews Microbiology* 1 (2018) doi:10.1038/s41579-018-0076-2.
862 14. Dombrowski, N., Lee, J.-H., Williams, T. A., Offre, P. & Spang, A. Genomic diversity, lifestyles and evolutionary
863 origins of DPANN archaea. *FEMS Microbiol Lett* **366**, (2019).
864 15. Huber, H. *et al.* A new phylum of Archaea represented by a nanosized hyperthermophilic symbiont. *Nature*
865 **417**, 63–67 (2002).
866 16. Jahn, U. *et al.* Nanoarchaeum equitans and Ignicoccus hospitalis: New insights into a unique, intimate
867 association of two Archaea. *J. Bacteriol.* **190**, 1743–1750 (2008).
868 17. Munson-McGee, J. H. *et al.* Nanoarchaeota, their Sulfolobales host, and Nanoarchaeota Virus distribution
869 across Yellowstone National Park Hot Springs. *Appl. Environ. Microbiol.* **81**, 7860–7868 (2015).
870 18. Wurch, L. *et al.* Genomics-informed isolation and characterization of a symbiotic Nanoarchaeota system
871 from a terrestrial geothermal environment. *Nature Communications* **7**, 12115 (2016).
872 19. Jarett, J. K. *et al.* Single-cell genomics of co-sorted Nanoarchaeota suggests novel putative host associations
873 and diversification of proteins involved in symbiosis. *Microbiome* **6**, 161 (2018).
874 20. John, E. S., Flores, G. E., Meneghin, J. & Reysenbach, A.-L. Deep-sea hydrothermal vent metagenome-
875 assembled genomes provide insight into the phylum Nanoarchaeota. *Environmental Microbiology Reports*
876 **11**, 262–270 (2019).
877 21. Golyshina, O. V. *et al.* 'ARMAN' archaea depend on association with euryarchaeal host in culture and in situ.
878 *Nature Communications* **8**, 60 (2017).

879 22. Krause, S., Bremges, A., Münch, P. C., McHardy, A. C. & Gescher, J. Characterisation of a stable laboratory co-
880 culture of acidophilic nanoorganisms. *Scientific Reports* **7**, 3289 (2017).
881 23. Hamm, J. N. *et al.* Unexpected host dependency of Antarctic Nanohaloarchaeota. *PNAS* 201905179 (2019)
882 doi:10.1073/pnas.1905179116.
883 24. Probst, A. J. *et al.* Differential depth distribution of microbial function and putative symbionts through
884 sediment-hosted aquifers in the deep terrestrial subsurface. *Nature Microbiology* 1 (2018)
885 doi:10.1038/s41564-017-0098-y.
886 25. Schwank, K. *et al.* An archaeal symbiont-host association from the deep terrestrial subsurface. *The ISME*
887 *Journal* 1 (2019) doi:10.1038/s41396-019-0421-0.
888 26. Brochier, C., Gribaldo, S., Zivanovic, Y., Confalonieri, F. & Forterre, P. Nanoarchaea: representatives of a
889 novel archaeal phylum or a fast-evolving euryarchaeal lineage related to Thermococcales? *Genome Biol* **6**,
890 R42 (2005).
891 27. Williams, T. A. *et al.* Integrative modeling of gene and genome evolution roots the archaeal tree of life. *PNAS*
892 201618463 (2017) doi:10.1073/pnas.1618463114.
893 28. Aouad, M. *et al.* Extreme halophilic archaea derive from two distinct methanogen Class II lineages. *Molecular*
894 *Phylogenetics and Evolution* **127**, 46–54 (2018).
895 29. Petitjean, C., Deschamps, P., López-García, P. & Moreira, D. Rooting the domain Archaea by phylogenomic
896 analysis supports the foundation of the new kingdom Proteoarchaeota. *Genome Biol Evol* **7**, 191–204 (2015).
897 30. Probst, A. J. *et al.* Biology of a widespread uncultivated archaeon that contributes to carbon fixation in the
898 subsurface. *Nature Communications* **5**, 5497 (2014).
899 31. Bird, J. T., Baker, B. J., Probst, A. J., Podar, M. & Lloyd, K. G. Culture independent genomic comparisons
900 reveal environmental adaptations for Altiarchaeales. *Front Microbiol* **7**, (2016).
901 32. Bergsten, J. A review of long-branch attraction. *Cladistics* **21**, 163–193 (2005).
902 33. Jeffroy, O., Brinkmann, H., Delsuc, F. & Philippe, H. Phylogenomics: the beginning of incongruence? *Trends in*
903 *Genetics* **22**, 225–231 (2006).
904 34. Moran, N. A. Accelerated evolution and Muller's rachet in endosymbiotic bacteria. *PNAS* **93**, 2873–2878
905 (1996).
906 35. Silva, F. J. & Santos-Garcia, D. Slow and fast evolving endosymbiont lineages: Positive correlation between
907 the rates of synonymous and non-synonymous substitution. *Front. Microbiol.* **6**, (2015).
908 36. Pollock, D. D., Zwickl, D. J., McGuire, J. A. & Hillis, D. M. Increased taxon sampling Is advantageous for
909 phylogenetic inference. *Syst Biol* **51**, 664–671 (2002).
910 37. Lartillot, N., Brinkmann, H. & Philippe, H. Suppression of long-branch attraction artefacts in the animal
911 phylogeny using a site-heterogeneous model. *BMC Evolutionary Biology* **7**, S4 (2007).
912 38. Pisani, D. Identifying and removing fast-evolving sites using compatibility analysis: An example from the
913 Arthropoda. *Syst Biol* **53**, 978–989 (2004).

914 39. Podar, M. *et al.* A genomic analysis of the archaeal system Ignicoccus hospitalis-Nanoarchaeum equitans.
915 *Genome Biology* **9**, R158 (2008).
916 40. Tully, B. J., Graham, E. D. & Heidelberg, J. F. The reconstruction of 2,631 draft metagenome-assembled
917 genomes from the global oceans. *Sci Data* **5**, 1–8 (2018).
918 41. Parks, D. H. *et al.* Recovery of nearly 8,000 metagenome-assembled genomes substantially expands the tree
919 of life. *Nature Microbiology* 1 (2017) doi:10.1038/s41564-017-0012-7.
920 42. Anantharaman, K. *et al.* Thousands of microbial genomes shed light on interconnected biogeochemical
921 processes in an aquifer system. *Nature Communications* **7**, 13219 (2016).
922 43. Bergauer, K. *et al.* Organic matter processing by microbial communities throughout the Atlantic water
923 column as revealed by metaproteomics. *PNAS* **115**, E400–E408 (2018).
924 44. Sunagawa, S. *et al.* Structure and function of the global ocean microbiome. *Science* **348**, 1261359 (2015).
925 45. Haro-Moreno, J. M. *et al.* Fine metagenomic profile of the Mediterranean stratified and mixed water
926 columns revealed by assembly and recruitment. *Microbiome* **6**, 128 (2018).
927 46. Bowers, R. M. *et al.* Minimum information about a single amplified genome (MISAG) and a metagenome-
928 assembled genome (MIMAG) of bacteria and archaea. *Nat Biotech* **35**, 725–731 (2017).
929 47. Parks, D. H. *et al.* A standardized bacterial taxonomy based on genome phylogeny substantially revises the
930 tree of life. *Nature Biotechnology* (2018) doi:10.1038/nbt.4229.
931 48. Darling, A. E. *et al.* PhyloSift: phylogenetic analysis of genomes and metagenomes. *PeerJ* **2**, e243 (2014).
932 49. Chaumeil, P.-A., Mussig, A. J., Hugenholtz, P. & Parks, D. H. GTDB-Tk: a toolkit to classify genomes with the
933 Genome Taxonomy Database. *Bioinformatics* (2019) doi:10.1093/bioinformatics/btz848.
934 50. Nguyen, L.-T., Schmidt, H. A., Haeseler, A. von & Minh, B. Q. IQ-TREE: A Fast and Effective Stochastic
935 Algorithm for Estimating Maximum-Likelihood Phylogenies. *Mol Biol Evol* **32**, 268–274 (2015).
936 51. Lartillot, N., Rodrigue, N., Stubbs, D. & Richer, J. PhyloBayes MPI: Phylogenetic reconstruction with infinite
937 mixtures of profiles in a parallel environment. *Syst Biol* **62**, 611–615 (2013).
938 52. Wilkinson, M., McInerney, J. O., Hirt, R. P., Foster, P. G. & Embley, T. M. Of clades and clans: terms for
939 phylogenetic relationships in unrooted trees. *Trends in Ecology & Evolution* **22**, 114–115 (2007).
940 53. Foster, P. G. & Hickey, D. A. Compositional bias may affect both DNA-based and protein-based phylogenetic
941 reconstructions. *J Mol Evol* **48**, 284–290 (1999).
942 54. Foster, P. G. Modeling compositional heterogeneity. *Syst Biol* **53**, 485–495 (2004).
943 55. Sorokin, D. Y. *et al.* Discovery of anaerobic lithoheterotrophic haloarchaea, ubiquitous in hypersaline
944 habitats. *The ISME Journal* **11**, 1245–1260 (2017).
945 56. Aouad, M., Borrel, G., Brochier-Armanet, C. & Gribaldo, S. Evolutionary placement of
946 Methanonatronarchaeia. *Nature Microbiology* **4**, 558 (2019).
947 57. Minh, B. Q. *et al.* IQ-TREE 2: New models and efficient methods for phylogenetic inference in the genomic
948 era. *Mol Biol Evol* doi:10.1093/molbev/msaa015.

949 58. Hoang, D. T., Chernomor, O., von Haeseler, A., Minh, B. Q. & Vinh, L. S. UFBoot2: Improving the Ultrafast
950 Bootstrap Approximation. *Mol Biol Evol* **35**, 518–522 (2018).
951 59. Guindon, S. *et al.* New Algorithms and Methods to Estimate Maximum-Likelihood Phylogenies: Assessing the
952 Performance of PhyML 3.0. *Syst Biol* **59**, 307–321 (2010).
953 60. Evguenieva-Hackenberg, E., Hou, L., Glaeser, S. & Klug, G. Structure and function of the archaeal exosome.
954 *Wiley Interdisciplinary Reviews: RNA* **5**, 623–635 (2014).
955 61. Bocquier, A. A. *et al.* Archaeal primase: bridging the gap between RNA and DNA polymerases. *Current*
956 *Biology* **11**, 452–456 (2001).
957 62. Raymann, K., Forterre, P., Brochier-Armanet, C. & Gribaldo, S. Global phylogenomic analysis disentangles the
958 complex evolutionary history of DNA replication in Archaea. *Genome Biol Evol* **6**, 192–212 (2014).
959 63. Oren, A. Pyruvate: a key nutrient in hypersaline environments? *Microorganisms* **3**, 407–416 (2015).
960 64. Sato, T., Atomi, H. & Imanaka, T. Archaeal type III RuBisCOs function in a pathway for AMP metabolism.
961 *Science* **315**, 1003–1006 (2007).
962 65. Aono, R., Sato, T., Imanaka, T. & Atomi, H. A pentose bisphosphate pathway for nucleoside degradation in
963 Archaea. *Nature Chemical Biology* **11**, 355–360 (2015).
964 66. Wrighton, K. C. *et al.* RubisCO of a nucleoside pathway known from Archaea is found in diverse uncultivated
965 phyla in bacteria. *ISME J* **10**, 2702–2714 (2016).
966 67. Jaffe, A. L., Castelle, C. J., Dupont, C. L. & Banfield, J. F. Lateral gene transfer shapes the distribution of
967 RuBisCO among Candidate Phyla Radiation bacteria and DPANN archaea. *Mol Biol Evol* **36**, 435–446 (2019).
968 68. Mulcahy, H., Charron-Mazenod, L. & Lewenza, S. Pseudomonas aeruginosa produces an extracellular
969 deoxyribonuclease that is required for utilization of DNA as a nutrient source. *Environmental Microbiology*
970 **12**, 1621–1629 (2010).
971 69. Chimileski, S., Dolas, K., Naor, A., Gophna, U. & Papke, R. T. Extracellular DNA metabolism in Haloferax
972 volcanii. *Frontiers in Microbiology* **5**, (2014).
973 70. Say, R. F. & Fuchs, G. Fructose 1,6-bisphosphate aldolase/phosphatase may be an ancestral gluconeogenic
974 enzyme. *Nature* **464**, 1077–1081 (2010).
975 71. Villanueva, L., Schouten, S. & Damsté, J. S. S. Phylogenomic analysis of lipid biosynthetic genes of Archaea
976 shed light on the 'lipid divide'. *Environ Microbiol* **19**, 54–69 (2017).
977 72. Waters, E. *et al.* The genome of Nanoarchaeum equitans: Insights into early archaeal evolution and derived
978 parasitism. *Proc Natl Acad Sci U S A* **100**, 12984–12988 (2003).
979 73. Jahn, U., Summons, R., Sturt, H., Grosjean, E. & Huber, H. Composition of the lipids of Nanoarchaeum
980 equitans and their origin from its host Ignicoccus sp. strain KIN4/I. *Arch Microbiol* **182**, 404–413 (2004).
981 74. Chen, L.-X. *et al.* Metabolic versatility of small archaea Micrarchaeota and Parvarchaeota. *The ISME Journal*
982 **12**, 756–775 (2018).

983 75. Probst, A. J. & Moissl-Eichinger, C. “Altiarchaeales”: Uncultivated Archaea from the Subsurface. *Life (Basel)* **5**,
984 1381–1395 (2015).
985 76. Youssef, N. H. *et al.* Insights into the metabolism, lifestyle and putative evolutionary history of the novel
986 archaeal phylum ‘Diapherotrites’’’. *ISME J* **9**, 447–460 (2015).
987 77. Moissl, C., Rudolph, C. & Huber, R. Natural communities of novel Archaea and Bacteria with a string-of-
988 pearls-like morphology: Molecular analysis of the Bacterial partners. *Appl Environ Microbiol* **68**, 933–937
989 (2002).
990 78. Moissl, C., Rudolph, C., Rachel, R., Koch, M. & Huber, R. In situ growth of the novel SM1 euryarchaeon from a
991 string-of-pearls-like microbial community in its cold biotope, its physical separation and insights into its
992 structure and physiology. *Arch Microbiol* **180**, 211–217 (2003).
993 79. Quinn, T. P., Richardson, M. F., Lovell, D. & Crowley, T. M. propr: An R-package for identifying proportionally
994 abundant features using compositional data analysis. *Scientific Reports* **7**, 1–9 (2017).
995 80. Hamann, E. *et al.* Syntrophic linkage between predatory Carpediemonas and specific prokaryotic
996 populations. *ISME J* **11**, 1205–1217 (2017).
997 81. Narasingarao, P. *et al.* De novo metagenomic assembly reveals abundant novel major lineage of Archaea in
998 hypersaline microbial communities. *ISME J* **6**, 81–93 (2012).
999 82. Williams, T. A. & Embley, T. M. Archaeal “Dark Matter” and the origin of Eukaryotes. *Genome Biol Evol* **6**,
1000 474–481 (2014).
1001 83. Li, D., Liu, C.-M., Luo, R., Sadakane, K. & Lam, T.-W. MEGAHIT: an ultra-fast single-node solution for large and
1002 complex metagenomics assembly via succinct de Bruijn graph. *Bioinformatics* **31**, 1674–1676 (2015).
1003 84. Li, H. Aligning sequence reads, clone sequences and assembly contigs with BWA-MEM. (2013).
1004 85. Kang, D. D., Froula, J., Egan, R. & Wang, Z. MetaBAT, an efficient tool for accurately reconstructing single
1005 genomes from complex microbial communities. *PeerJ* **3**, e1165 (2015).
1006 86. Parks, D. H., Imelfort, M., Skennerton, C. T., Hugenholtz, P. & Tyson, G. W. CheckM: assessing the quality of
1007 microbial genomes recovered from isolates, single cells, and metagenomes. *Genome Research* **25**, 1043–
1008 1055 (2015).
1009 87. Buchfink, B., Xie, C. & Huson, D. H. Fast and sensitive protein alignment using DIAMOND. *Nature Methods*
1010 **12**, 59–60 (2015).
1011 88. Katoh, K., Misawa, K., Kuma, K. & Miyata, T. MAFFT: a novel method for rapid multiple sequence alignment
1012 based on fast Fourier transform. *Nucl. Acids Res.* **30**, 3059–3066 (2002).
1013 89. Criscuolo, A. & Gribaldo, S. BMGE (Block Mapping and Gathering with Entropy): a new software for selection
1014 of phylogenetic informative regions from multiple sequence alignments. *BMC Evol Biol* **10**, 210 (2010).
1015 90. St. John, E. *et al.* A New Symbiotic Nanoarchaeote (Candidatus Nanoclepta minutus) and its Host
1016 (Zestosphaera tikiterensis gen. nov., sp. nov.) from a New Zealand Hot Spring. *Systematic and Applied*
1017 *Microbiology* (2018) doi:10.1016/j.syapm.2018.08.005.

1018 91. Prokofeva, M. I. *et al.* Isolation of the anaerobic thermoacidophilic crenarchaeote Acidilobus saccharovorans
1019 sp. nov. and proposal of Acidilobales ord. nov., including Acidilobaceae fam. nov. and Caldisphaeraceae fam.
1020 nov. *International Journal of Systematic and Evolutionary Microbiology,* **59**, 3116–3122 (2009).
1021 92. Altenhoff, A. M. *et al.* OMA standalone: orthology inference among public and custom genomes and
1022 transcriptomes. *Genome Res.* (2019) doi:10.1101/gr.243212.118.
1023 93. Eddy, S. R. A new generation of homology search tools based on probabilistic inference. in *Genome*
1024 *Informatics 2009* 205–211 (PUBLISHED BY IMPERIAL COLLEGE PRESS AND DISTRIBUTED BY WORLD
1025 SCIENTIFIC PUBLISHING CO., 2009). doi:10.1142/9781848165632_0019.
1026 94. Susko, E. & Roger, A. J. On reduced amino acid alphabets for phylogenetic inference. *Mol Biol Evol* **24**, 2139–
1027 2150 (2007).
1028 95. Kostka, M., Uzlikova, M., Cepicka, I. & Flegr, J. SlowFaster, a user-friendly program for slow-fast analysis and
1029 its application on phylogeny of Blastocystis. *BMC Bioinformatics* **9**, 341 (2008).
1030 96. Finn, R. D., Clements, J. & Eddy, S. R. HMMER web server: interactive sequence similarity searching. *Nucleic*
1031 *Acids Res* **39**, W29–W37 (2011).
1032 97. Price, M. N., Dehal, P. S. & Arkin, A. P. FastTree 2 – Approximately Maximum-Likelihood Trees for Large
1033 Alignments. *PLOS ONE* **5**, e9490 (2010).
1034 98. Tria, F. D. K., Landan, G. & Dagan, T. Phylogenetic rooting using minimal ancestor deviation. *Nature Ecology*
1035 *& Evolution* **1**, 1–7 (2017).
1036 99. Brown, C. T. *et al.* Unusual biology across a group comprising more than 15% of domain Bacteria. *Nature*
1037 **523**, 208–211 (2015).
1038 100. Philippe, H., Zhou, Y., Brinkmann, H., Rodrigue, N. & Delsuc, F. Heterotachy and long-branch attraction in
1039 phylogenetics. *BMC Evol Biol* **5**, 50 (2005).
1040 101. Brochier, C. & Philippe, H. A non-hyperthermophilic ancestor for Bacteria. *Nature* **417**, 244–244 (2002).
1041 102. Makarova, K. S., Wolf, Y. I. & Koonin, E. V. Archaeal Clusters of Orthologous Genes (arCOGs): An update and
1042 application for analysis of shared features between Thermococcales, Methanococcales, and
1043 Methanobacteriales. *Life* **5**, 818–840 (2015).
1044 103. Seemann, T. barrnap 0.9 : rapid ribosomal RNA prediction. *https://github.com/tseemann/barrnap*.
1045 104. Quinlan, A. R. & Hall, I. M. BEDTools: a flexible suite of utilities for comparing genomic features.
1046 *Bioinformatics* **26**, 841–842 (2010).
1047 105. Capella-Gutiérrez, S., Silla-Martínez, J. M. & Gabaldón, T. trimAl: a tool for automated alignment trimming in
1048 large-scale phylogenetic analyses. *Bioinformatics* **25**, 1972–1973 (2009).
1049 106. Tareen, A. & Kinney, J. B. Logomaker: beautiful sequence logos in Python. *Bioinformatics* (2019)
1050 doi:10.1093/bioinformatics/btz921.
1051 107. Seemann, T. Prokka: rapid prokaryotic genome annotation. *Bioinformatics* **30**, 2068–2069 (2014).

1052 108. Aramaki, T. *et al.* KofamKOALA: KEGG ortholog assignment based on profile HMM and adaptive score
1053 threshold. *bioRxiv* 602110 (2019) doi:10.1101/602110.
1054 109. Bateman, A. *et al.* The Pfam protein families database. *Nucleic Acids Res* **32**, D138–D141 (2004).
1055 110. Haft, D. H., Selengut, J. D. & White, O. The TIGRFAMs database of protein families. *Nucleic Acids Res* **31**, 371–
1056 373 (2003).
1057 111. Cantarel, B. L. *et al.* The Carbohydrate-Active EnZymes database (CAZy): an expert resource for
1058 Glycogenomics. *Nucl. Acids Res.* **37**, D233–D238 (2009).
1059 112. Rawlings, N. D., Barrett, A. J. & Finn, R. Twenty years of the MEROPS database of proteolytic enzymes, their
1060 substrates and inhibitors. *Nucl. Acids Res.* **44**, D343–D350 (2016).
1061 113. Saier, M. H., Tran, C. V. & Barabote, R. D. TCDB: the Transporter Classification Database for membrane
1062 transport protein analyses and information. *Nucleic Acids Res* **34**, D181–D186 (2006).
1063 114. Søndergaard, D., Pedersen, C. N. S. & Greening, C. HydDB: A web tool for hydrogenase classification and
1064 analysis. *Scientific Reports* **6**, 34212 (2016).
1065 115. Jones, P. *et al.* InterProScan 5: genome-scale protein function classification. *Bioinformatics* **30**, 1236–1240
1066 (2014).
1067 116. Altschul, S. F. *et al.* Gapped BLAST and PSI-BLAST: a new generation of protein database search programs.
1068 *Nucl. Acids Res.* **25**, 3389–3402 (1997).
1069 117. Lowe, T. M. & Eddy, S. R. tRNAscan-SE: a program for improved detection of transfer RNA genes in genomic
1070 sequence. *Nucleic Acids Res* **25**, 955–964 (1997).
1071 118. Steinegger, M. *et al.* HH-suite3 for fast remote homology detection and deep protein annotation. *BMC*
1072 *Bioinformatics* **20**, 473 (2019).
1073 119. Kelley, L. A., Mezulis, S., Yates, C. M., Wass, M. N. & Sternberg, M. J. E. The Phyre2 web portal for protein
1074 modeling, prediction and analysis. *Nat Protoc* **10**, 845–858 (2015).
1075 120. Parks, D. *A toolbox for comparative genomics. Contribute to dparks1134/CompareM development by*
1076 *creating an account on GitHub*. (2019).
1077 121. Bray, N. L., Pimentel, H., Melsted, P. & Pachter, L. Near-optimal probabilistic RNA-seq quantification. *Nature*
1078 *Biotechnology* **34**, 525–527 (2016).
1079
1080

Table 1

		General Stats										CheckM statistics									
BinID	Order	Habitat	Length (MB)	GC (%)	Contig (bp)	nr. of contigs	nr. of proteins	16 S	23 S	5 S	tRNA count	Nr. of markers	0	1	2	3	4	5+	Completeness (%)	Contamination (%)	Heterogeneity (%)
SRR2090153.bin1042	Naiadarchaeales	Aquifer	0.72	37.7	12,286	144	809				15	149 (142)	61 (54)	87	1	0	0	0	65.0 (69.1)	0.93 (1.0)	0
SRR2090153.bin461	Naiadarchaeales	Aquifer	0.68	43.0	11,937	152	787				17	149 (142)	76 (69)	69	4	0	0	0	55.0 (58.6)	3.7 (3.92)	50
SRR2090159.bin1129*	**Naiadarchaeales**	**Aquifer**	**0.98**	**37.9**	**97,397**	**52**	**1081**		**1**	**1**	**21**	**149 (142)**	**11 (4)**	**135**	**3**	**0**	**0**	**0**	**90.7 (96.0)**	**2.8 (2.9)**	**0**
SRR2090159.bin1288	Naiadarchaeales	Aquifer	0.70	43.0	19,705	102	821				17	150 (142)	63 (56)	82	4	0	0	0	65.1 (69.3)	3.7 (3.9)	75
GCA_002502135.1	Undinarchaeales	Marine	0.73	39.5	74,625	23	819	1	1	1	19	151 (142)	23 (16)	126	0	0	0	0	79.9 (84.3)	0 (0)	0
GCA_002494525.1	Undinarchaeales	Marine	0.64	40.7	145,584	11	706		1	1	21	152 (142)	12 (5)	137	0	0	0	0	89.7 (95.1)	0 (0)	0
GCA_002495465.1	Undinarchaeales	Marine	0.61	41.4	75,044	19	696		1	1	19	153 (142)	21 (14)	128	0	0	0	0	82.6 (87.6)	0 (0)	0
GCA_002501985.1	Undinarchaeales	Marine	0.61	40.8	118,101	22	678			1	21	154 (142)	14 (7)	135	0	0	0	0	87.9 (93.1)	0 (0)	0
GCA_002687935.1	Undinarchaeales	Marine	0.67	41.6	173,317	11	752	1	1	1	21	155 (142)	12 (5)	135	2	0	0	0	89.7 (95.1)	1.9 (2.0)	100
SRR4028224.bin17*	**Undinarchaeales**	**Marine**	**0.62**	**42.3**	**114,673**	**19**	**700**	**1**	**1**	**1**	**21**	**156 (142)**	**12 (5)**	**137**	**0**	**0**	**0**	**0**	**89.7 (95.1)**	**0 (0)**	**0**
SRR5007147.bin71	Undinarchaeales	Marine	0.62	42.0	54,083	39	705			1	21	157 (142)	17 (10)	132	0	0	0	0	87.2 (92.5)	0 (0)	0
U_76725	Undinarchaeales	Marine	0.37	40.2	12,036	80	416				13	158 (142)	76 (69)	72	1	0	0	0	54.4 (58.1)	0.93 (1.0)	100

Figure 1

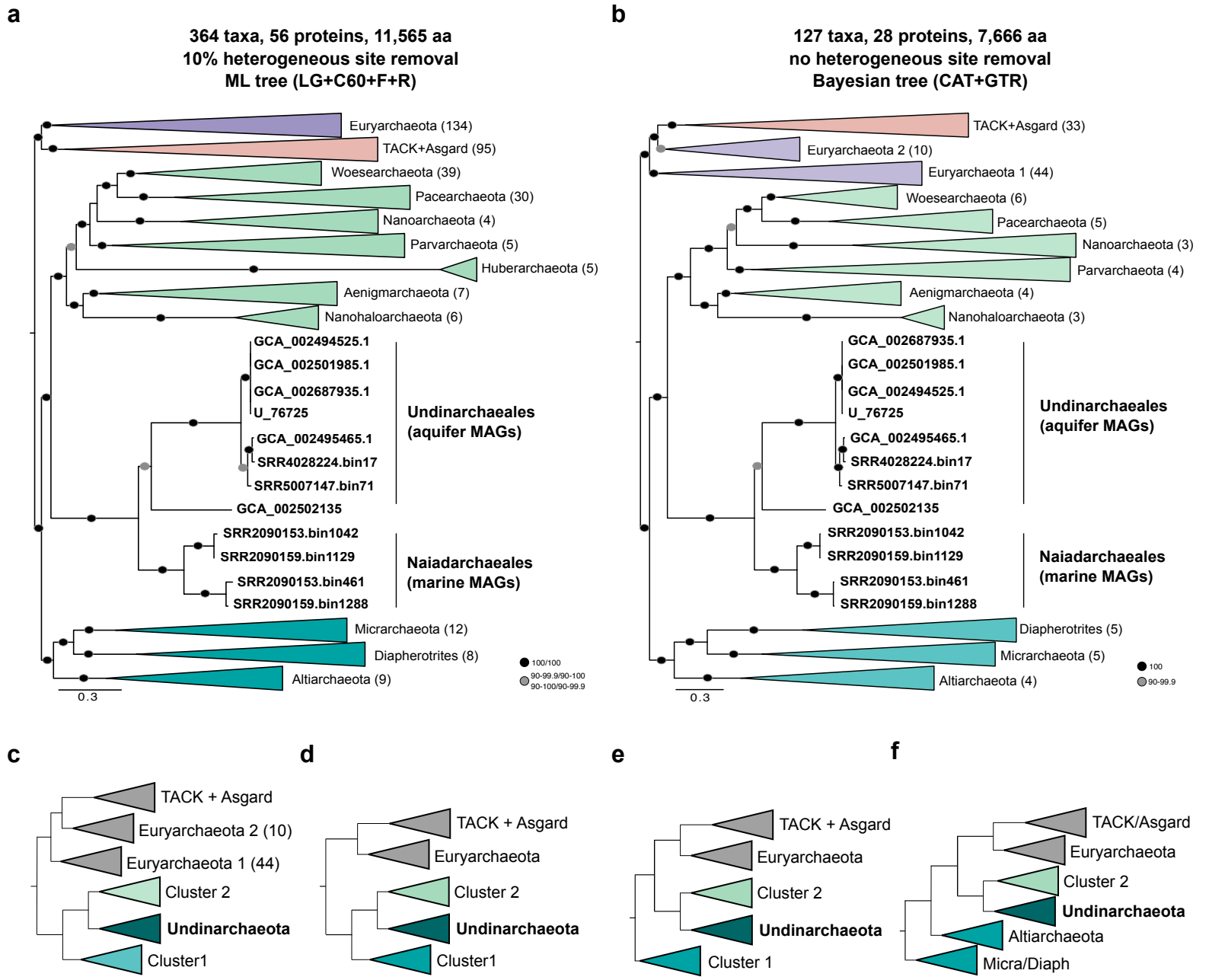
a
364 taxa, 56 proteins, 11,565 aa
10% heterogeneous site removal
ML tree (LG+C60+F+R)
Euryarchaeota (134)
TACK+Asgard (95)
Woesearchaeota (39)
Pacearchaeota (30)
Nanoarchaeota (4)
Parvarchaeota (5)
Huberarchaeota (5)
Aenigmarchaeota (7)
Nanohaloarchaeota (6)
GCA_002494525.1
GCA_002501985.1
GCA_002687935.1
U_76725
GCA_002495465.1
SRR4028224.bin17
SRR5007147.bin71
GCA_002502135
Undinarchaeales
(aquifer MAGs)
SRR2090153.bin1042
SRR2090159.bin1129
SRR2090153.bin461
SRR2090159.bin1288
Naiadarchaeales
(marine MAGs)
Micrarchaeota (12)
Diapherotrites (8)
Altiarchaeota (9)
0.3
100/100
90-99.9/90-100
90-100/90-99.9
b
127 taxa, 28 proteins, 7,666 aa
no heterogeneous site removal
Bayesian tree (CAT+GTR)
TACK+Asgard (33)
Euryarchaeota 2 (10)
Euryarchaeota 1 (44)
Woesearchaeota (6)
Pacearchaeota (5)
Nanoarchaeota (3)
Parvarchaeota (4)
Aenigmarchaeota (4)
Nanohaloarchaeota (3)
GCA_002687935.1
GCA_002501985.1
GCA_002494525.1
U_76725
GCA_002495465.1
SRR4028224.bin17
SRR5007147.bin71
GCA_002502135
Undinarchaeales
(aquifer MAGs)
SRR2090153.bin1042
SRR2090159.bin1129
SRR2090153.bin461
SRR2090159.bin1288
Naiadarchaeales
(marine MAGs)
Diapherotrites (5)
Micrarchaeota (5)
Altiarchaeota (4)
0.3
100
90-99.9
c
TACK + Asgard
Euryarchaeota 2 (10)
Euryarchaeota 1 (44)
Cluster 2
Undinarchaeota
Cluster1
d
TACK + Asgard
Euryarchaeota
Cluster 2
Undinarchaeota
Cluster1
e
TACK + Asgard
Euryarchaeota
Cluster 2
Undinarchaeota
Cluster 1
f
TACK/Asgard
Euryarchaeota
Cluster 2
Undinarchaeota
Altiarchaeota
Micra/Diaph

Figure 2

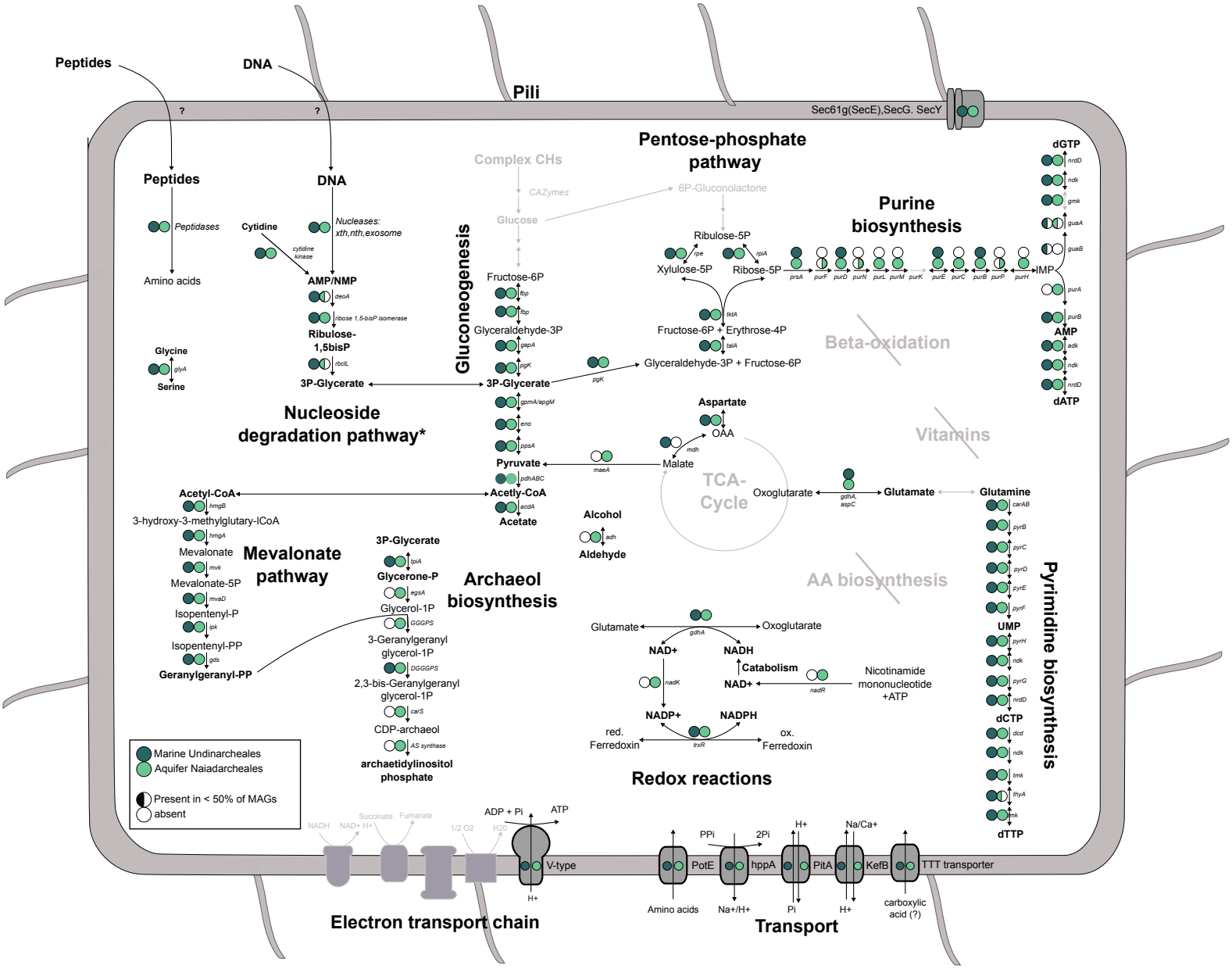
Peptides
DNA
Pili
Sec61g(SecE),SecG. SecY
Peptides
Peptidases
Amino acids
DNA
Nucleases: xth,nth,exosome
Cytidine
cytidine kinase
AMP/NMP
deoA
ribose 1,5-bisP isomerase
Ribulose-1,5bisP
rbcIL
3P-Glycerate
Glycine
glyA
Serine
Nucleoside degradation pathway*
Complex CHs
CAZymes
Glucose
Gluconeogenesis
Fructose-6P
fbp
fbp
Glyceraldehyde-3P
gapA
pgK
3P-Glycerate
gpmA/apgM
eno
ppsA
Pyruvate
pdhABC
Acetly-CoA
acdA
Acetate
Pentose-phosphate pathway
6P-Gluconolactone
Ribulose-5P
rpe
rpiA
Xylulose-5P
Ribose-5P
tktA
Fructose-6P + Erythrose-4P
talA
Glyceraldehyde-3P + Fructose-6P
pgK
Purine biosynthesis
prsA
purF purD purN purL purM purK
purE purC purB purP purH
IMP
purA
purB
AMP
adk
ndk
nrdD
dATP
dGTP
nrdD
ndk
gmk
guaA
guaB
Beta-oxidation
Vitamins
Aspartate
OAA
mdh
Malate
maeA
TCA-Cycle
Oxoglutarate
gdhA, aspC
Glutamate
Glutamine
carAB
pyrB
pyrC
pyrD
pyrE
pyrF
UMP
pyrH
ndk
pyrG
nrdD
dCTP
dcd
ndk
tmk
thyA
tmk
dTTP
Pyrimidine biosynthesis
Acetyl-CoA
hmgB
3-hydroxy-3-methylglutary-lCoA
hmgA
Mevalonate
mvk
Mevalonate-5P
mvaD
Isopentenyl-P
ipk
Isopentenyl-PP
gds
Geranylgeranyl-PP
Mevalonate pathway
Alcohol
adh
Aldehyde
3P-Glycerate
tpiA
Glycerone-P
egsA
Glycerol-1P
GGGPS
3-Geranylgeranyl glycerol-1P
DGGGPS
2,3-bis-Geranylgeranyl glycerol-1P
carS
CDP-archaeol
AS synthase
archaetidylinositol phosphate
Archaeol biosynthesis
AA biosynthesis
Glutamate
gdhA
Oxoglutarate
NAD+
NADH
Catabolism
NAD+
nadK
nadR
Nicotinamide mononucleotide +ATP
NADP+
NADPH
red. Ferredoxin
trxR
ox. Ferredoxin
Redox reactions
Marine Undinarcheales
Aquifer Naiadarcheales
Present in < 50% of MAGs
absent
NADH
NAD+ H+
Succinate
Fumarate
1/2 O2
H2O
ADP + Pi
ATP
V-type
H+
Electron transport chain
PPi
2Pi
H+
Na/Ca+
PotE
hppA
PitA
KefB
TTT transporter
Amino acids
Na+/H+
Pi
H+
carboxylic acid (?)
Transport

Figure 3

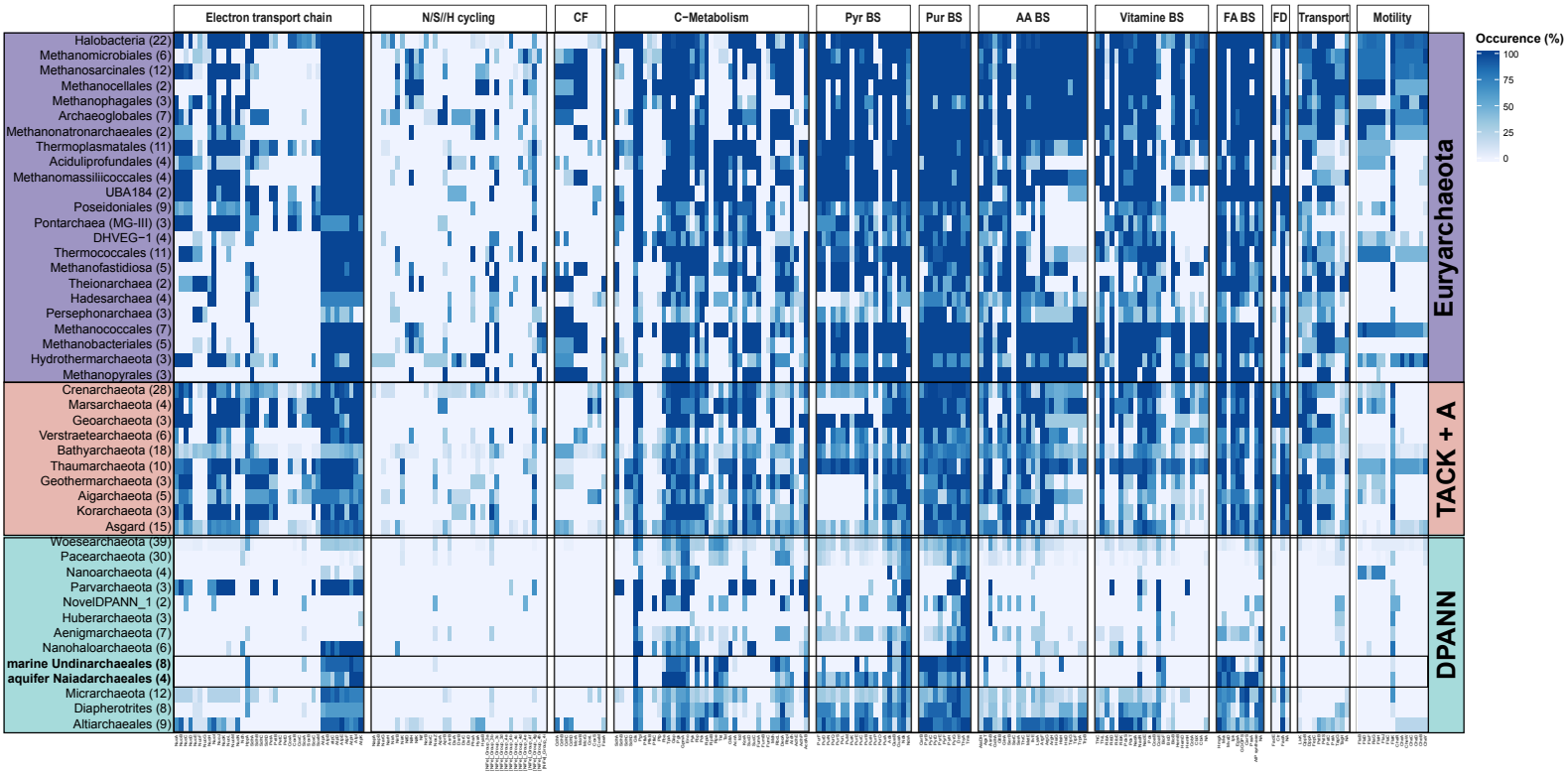
Electron transport chain
N/S//H cycling
CF
C−Metabolism
Pyr BS
Pur BS
AA BS
Vitamine BS
FA BS
FD
Transport
Motility
Occurence (%)
100
75
50
25
0
Halobacteria (22)
Methanomicrobiales (6)
Methanosarcinales (12)
Methanocellales (2)
Methanophagales (3)
Archaeoglobales (7)
Methanonatronarchaeales (2)
Thermoplasmatales (11)
Aciduliprofundales (4)
Methanomassiliicoccales (4)
UBA184 (2)
Poseidoniales (9)
Pontarchaea (MG-III) (3)
DHVEG−1 (4)
Thermococcales (11)
Methanofastidiosa (5)
Theionarchaea (2)
Hadesarchaea (4)
Persephonarchaea (3)
Methanococcales (7)
Methanobacteriales (5)
Hydrothermarchaeota (3)
Methanopyrales (3)
Euryarchaeota
Crenarchaeota (28)
Marsarchaeota (4)
Geoarchaeota (3)
Verstraetearchaeota (6)
Bathyarchaeota (18)
Thaumarchaeota (10)
Geothermarchaeota (3)
Aigarchaeota (5)
Korarchaeota (3)
Asgard (15)
TACK + A
Woesearchaeota (39)
Pacearchaeota (30)
Nanoarchaeota (4)
Parvarchaeota (3)
NovelDPANN_1 (2)
Huberarchaeota (3)
Aenigmarchaeota (7)
Nanohaloarchaeota (6)
marine Undinarchaeales (8)
aquifer Naiadarchaeales (4)
Micrarchaeota (12)
Diapherotrites (8)
Altiarchaeales (9)
DPANN

Figure 4

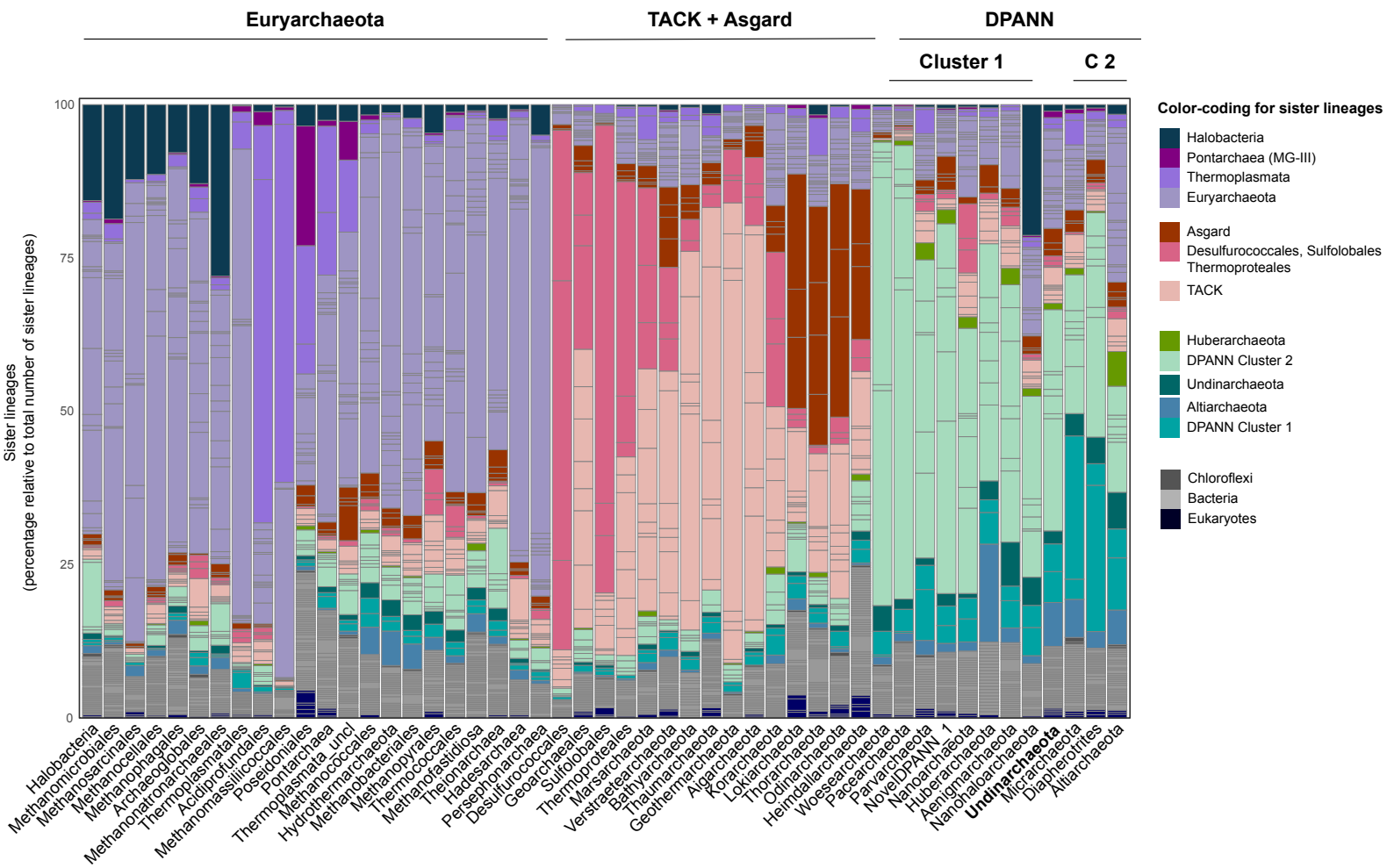

Phylogenetic relationships of undinarchaeal core proteins across archaeal clades of interest